19

Satellite Atmospheres

Melissa A. McGrath
Space Telescope Science Institute

Emmanuel Lellouch
Observatoire de Paris

Darrell F. Strobel, Paul D. Feldman
The Johns Hopkins University

Robert E. Johnson
University of Virginia

19.1 INTRODUCTION

Study of the Galilean satellite atmospheres is a field that has blossomed in the 25 years since the last major retrospective of the jovian system (Gehrels 1976). At the time of that book, only one of these satellites, Io, was thought to possess an atmosphere, although a stellar occultation had suggested the possibility of a tenuous atmosphere on Ganymede as well (Carlson *et al.* 1973).

The discovery of the Io plasma torus (Kupo *et al.* 1976) and the in situ characterization of the plasma in the jovian magnetosphere by the *Voyager* spacecraft in 1979 made it clear that all of the Galilean satellites are exposed to a harsh radiation environment (see Chapter 23). The collisional impact of magnetospheric ions with these satellites erodes their surfaces and sputters atoms and molecules to create atmospheres and/or exospheres (see Chapter 20). Surface processes such as sublimation and active volcanoes contribute as well.

The discovery and confirmation that all these satellites possess tenuous atmospheres has been accomplished by three of NASA's largest and most productive space missions of the last 25 years: *Voyager*, Hubble Space Telescope (HST) and *Galileo*. Numerous ground-based observations have also contributed to the substantial advances in our understanding of these atmospheres. Whereas in 1975 two species (sodium and potassium) were known to be present on Io, today nine atomic and molecular species have been detected, and 2–4 species have also been detected at each of Europa, Ganymede and Callisto.

We present in this chapter a summary of our current knowledge about the atmospheres of Io, Europa, Ganymede, and Callisto, with a focus on the discoveries and progress made since 1990.

19.2 IO

19.2.1 Introduction and Early Studies

Our knowledge of Io's atmosphere has undergone a major revision in the last decade. Before 1990, observational information was restricted to several clear but indirect pieces of evidence, a single direct infrared detection by *Voyager* in 1979, and a number of upper limits from ultraviolet (UV) spectroscopy. Even loosely constrained, Io's atmosphere was quickly recognized as bearing unique features among planetary atmospheres, the most prominent being its apparent spatial and temporal variability. The lack of data did not hinder theoretical studies on the horizontal, vertical and chemical structure during the 1980s. Since 1990, the direct detection of it from Earth and Earth orbit in different wavelength ranges has provided a much firmer basis for our perception of Io's atmosphere. After a brief introduction, we concentrate in this section on recent developments. The earlier studies are detailed in previous reviews by Johnson and Matson (1989), Lellouch (1996), Spencer and Schneider (1996), and Trafton *et al.* (1998).

The first definite evidence for an atmosphere around Io was obtained in 1973 with the *Pioneer 10* detection of relatively dense ionospheric layers above Io's surface near the terminator (Kliore *et al.* 1974, 1975). Preliminary estimates of the neutral atmosphere required to explain these data yielded surface pressures of 10^{-8}–10^{-9} bars. Shortly after, optical observations detected atomic sodium around Io (Brown 1974), and it was quickly established that the observed sodium formed a cloud of atoms in orbit around Jupiter that had escaped non-thermally from Io, implying a source of Na in Io's atmosphere or at the surface. Further evidence for atmospheric escape was obtained from the optical detection of a potassium cloud (Trafton 1975) and of ionized sulfur in the jovian magnetosphere (Kupo *et al.* 1976).

The "watershed event" for Io's atmosphere occurred the

same year with a triple discovery: the presence of active volcanism on Io's surface (Morabito *et al.* 1979), the attribution of a 4.1 μm feature in Io's infrared (IR) spectrum to solid SO_2 (Fanale *et al.* 1979, Smythe *et al.* 1979), and the detection of gaseous SO_2 at 7.3 μm over the volcanic center Loki Patera (Pearl *et al.* 1979). The latter was interpreted as indicating a 100 nbar local atmosphere at 130 K, although a subsequent reinterpretation (Lellouch *et al.* 1992) has shown it to be consistent with lower pressures (5–40 nbar) and higher temperatures (up to 400 K). After this single observation, Io's SO_2 atmosphere eluded detection for another eleven years, although several attempts in the UV were useful in placing upper limits on the global SO_2 abundance, the most significant being that of Ballester *et al.* (1990) which placed an upper limit of $2 \times 10^{17}\,\mathrm{cm}^{-2}$ on a homogeneous SO_2 atmosphere.

After the *Voyager* flybys and until the detection of SO_2 rotational line emission by Lellouch *et al.* (1990), theorists had only three data sets to characterize the atmosphere of Io: the two *Pioneer 10* ionospheric radio occultation profiles and the detection of a volcanic plume over Loki by *Voyager* IRIS. A number of questions were raised: (1) how representative was the 100 nbar plume atmosphere of the whole atmosphere and how far would a plume atmosphere propagate horizontally? (2) was the atmosphere collisionally thin or collisionally thick to the penetration of thermal ions in the Io plasma torus as they swept by Io (if in the former, the atmosphere might be sputter generated)? and (3) did the *Pioneer 10* detection of "dayside" and "nightside" ionospheres imply a global atmosphere but with substantial day/night surface pressure variations? Since most of the SO_2 gas from volcanic vents eventually condenses on the surface, what fraction of Io's atmosphere was "buffered" by vapor pressure equilibrium with surface SO_2 frost/ice? These questions were pursued by modelers with limited success due to insufficient knowledge of the atmosphere, although two pieces of work in this period (McGrath and Johnson 1987, Schneider *et al.* 1991) did provide indirect evidence for an atmosphere with exobase above the surface (i.e., collisionally thick).

19.2.2 Recent Progress: Observations

SO_2 Atmosphere

Since the first detection of the SO_2 atmosphere via IR spectroscopy in 1979, two additional techniques have become important in characterizing the atmosphere in greater detail. The first is millimeter-wave spectroscopy, which detects SO_2 in emission. The second is UV observations (imaging and spectroscopy), which detect the SO_2 gas primarily in absorption. Advances in IR techniques have also enabled new SO_2 measurements from ground-based telescopes. We briefly describe the advances made since 1990 using these three techniques; results are also summarized in Table 19.1.

Millimeter Observations The first post-*Voyager* detection of SO_2 gas was made by Lellouch *et al.* (1990) using millimeter-wave heterodyne spectroscopy. The observations have been performed frequently since the initial detection, and yielded useful data in 1991, 1993, 1994, 1995, 1999, and 2002. To avoid contamination by Jupiter, the observations are conducted only near eastern or western elongation (orbital longitude $L = 90°$ or $L = 270°$ respectively), and they have low temporal (i.e., longitudinal) resolution and do not resolve the satellite spatially (10–20″ spatial resolution). Twelve SO_2 emission lines, which span a factor of ~20 in line intensity, have been detected, all but one with relatively low energy levels (8 to $165\,\mathrm{cm}^{-1}$). Because the rotational levels have very short collisional relaxation times, the observed transitions represent local thermodynamic equilibrium (LTE) thermal emission of the atmosphere at number densities as small as $\sim 2 \times 10^5\mathrm{cm}^{-3}$ (Lellouch *et al.* 1992). The strongest have brightness temperature contrasts of 20–40 K above the surface continuum, implying that the mean dayside SO_2 gas temperature is higher than the mean surface brightness temperature by at least 20–40 K, perhaps much more if the dayside atmosphere covers only a fraction of Io's surface and/or if the lines are not optically thick. The observed lines are fully resolved. The linewidth (FWHM) of the strongest lines is ~600 kHz at 220 GHz and scales as the line frequency, indicating Doppler broadening. Collisional broadening would imply an implausible 10^{-4} bar surface pressure. The FWHM/frequency line ratio of $\sim 2.7 \times 10^{-6}$ gives a temperature of 910 K for thermal broadening, or a velocity of $0.8\,\mathrm{km\,s}^{-1}$ for bulk velocity broadening. A sampling of the millimeter detections is shown in Figure 19.1.

The first interpretation (Lellouch *et al.* 1990, 1992) assumed that Io's SO_2 atmosphere is in hydrostatic equilibrium, in which case $T = 910$ K is an upper limit to the mean atmospheric temperature. Since the bulk of Io's atmosphere is likely to be at a much lower temperature (see discussion of radiative models below), the linewidths were interpreted as being affected by saturation effects. For reasonable values of the atmospheric temperatures, this indicated local column densities of $0.5\text{–}5 \times 10^{17}\,\mathrm{cm}^{-2}$ covering only a small fraction of the disk. A more precise characterization requires multiline observations, whereby the *relative* contrast of at least two lines with known intrinsic strengths constrains their respective saturation degree, thereby helping to disentangle the temperature/pressure/coverage variables. This method, which motivated most of the SO_2 millimeter-wave observations over 1991–1999, is not equivalent to a rotational diagram analysis because all lines have similar lower energy levels. The line optical depth can be derived from the data, yielding the SO_2 column density (or equivalently the surface pressure). Once this is obtained, the fraction of the projected surface (disk) covered by the atmosphere, f_p, is inferred from the absolute line contrast. Converting this to a hemispherical coverage f_h requires knowing how the gas is distributed. If the atmosphere is assumed to be restricted to a circular region around disk center, i.e., close to the subsolar point, f_h and f_p are related through $f_\mathrm{h} = 1 - (1 - f_\mathrm{p})^{1/2}$.

In 1991, the non-detection of the weaker 146.605 GHz line on the trailing side led Lellouch *et al.* (1992) to conclude that the detected 222.965 and 143.057 GHz lines had a moderate optical depth (~2). This in turn implied a hot (T_atm = 500–600 K), dense (3–15 nbar) and very localized (f_p = 5–8 %, f_h = 2.5–4 %) atmosphere. The high temperature and low areal extent for the trailing atmosphere were confirmed from the 1993 and 1994 observations (see Lellouch 1996). By contrast, the detection of the 146.605 GHz line on the leading side in March 1993 and May 1994 suggested a subtantially lower temperature (250–400 K) and higher extent (f_p = 12–

Table 19.1. Summary of SO_2 observations of Io since 1990.

Reference	Type	λ Coverage	$\Delta\lambda$	Date	Location	Spatial Resolution	Fractional coverage $\mathcal{N}$ (cm^{-2})	Fractional coverage T(K)	Fractional coverage %	Uniform coverage $\mathcal{N}$(cm^{-2})	Uniform coverage T(K)
(1) Lellouch *et al.* 1992	S	1.3–2 mm	100 kHz	1992	Trailing	none	$(1.5\text{–}7.5) \times 10^{17}$	500–600	2.5–4		
(2) Lellouch *et al.* 1996	S	1.3–2 mm	100 kHz	1993–94	Leading	none	$(1.5\text{–}2.5) \times 10^{17}$	250–400[a]	6–9		
							$0.8\text{–}2 \times 10^{17}$	(250)[b]	11–18		
					Trailing		$(2.5\text{–}7.5) \times 10^{17}$	600[a]	2.5–4		
							2×10^{16}	(250)[b]	29–36		
(3) Lellouch *et al.* 2000	S	1.3–2 mm	100 kHz	10/99	Lead.+Trail.	none	1.6×10^{17}	300[a]	10		
							8×10^{16}	(250)[b]	20		
(4) Lellouch *et al.* 2003	S	1.3–2 mm	100 kHz	01/02	Lead.+Trail.	none	6×10^{16}	140–250	18		
							5.5×10^{16}	180[b]	25		
(5) Ballester *et al.* 1994	S	1900–2300 Å	4.5Å	03/92	$L = 285°$	none	2×10^{17}	110	11	$(0.6\text{–}1) \times 10^{16}$	150–300
(6) Sartoretti *et al.* 1994	I	2325Å	±170Å	03/92		~200 km	$(5\text{–}7) \times 10^{17}$	(213)	3–20		
1996		2600Å	±182Å	06/93			$\sim 1 \times 10^{18}$		11–15		
		2850Å	±240Å	07/93							
(7) Clarke *et al.* 1994	S	2200–3300Å	12Å	01/92	$L = 4-31°$	none	2×10^{19}	(213)	10	$< 4 \times 10^{16}$	(213)
(8) Trafton *et al.* 1996	S	2097–2136Å	0.3Å	08/96	$L = 245-285°$	none	$<9.6 \times 10^{16}$	(213)	>23	7×10^{15}	(213)
					$L = 80-97°$		$<9.6 \times 10^{16}$		>20	5×10^{15}	
(9) Spencer *et al.* 1997	I	2740Å	±170Å	07/95	Pele plume		3.7×10^{17}(t) if	(213)	N/A		
		3365Å	±215Å	07/96			τ is all SO_2 gas				
(10) Hendrix *et al.* 1999	S	2100–3200Å	13.7Å	05/98	$L = 120° - 150°$	30° in long,	1×10^{19}	(213)	25		
						none in lat	4×10^{17}		35		
							0		40		
(11) McGrath *et al.* 2000a	S	1900–2300 Å	1.5Å	8/96	Pele	~750 km	3.25×10^{16}	280			
					Ra		1.5×10^{16}	150			
					"T3", 45°S, 300°W		7×10^{15}	200			
(12) Spencer *et al.* 2000	I	2740 3365Å		10/99	Pele plume		7×10^{16}(t)	(213)			
	S	2050–3100Å	3Å								
(13) Feldman *et al.* 2000a	I	1216Å	Monochro-	10/97	$L = 258°$	~200 km	3×10^{16}				
			matic	08/98	$L = 310°$		1.4×10^{16}				
				08/98	$L = 44°$		4.5×10^{16}				
(14) Jessup *et al.* 2004	S	2050–3150Å	6.5 Å	11/01	$L = 152°$, ±60° lat,	~200 km	~few $\times 10^{17}$,	100–450			
				12/01	centered on		(0–20)° lat				
					Prometheus		$\sim 1 \times 10^{16}$,				
							(40–50)° lat				
(15) Spencer *et al.* 2002	S	18.9 μm	$\lambda/\Delta\lambda$=	11/01	$L = 16°$	none				2×10^{16}	
			50 000		$L = 213°$					1×10^{17}	

Note that ( ) under T indicates that the temperature is *assumed*, not derived or inferred. [a]Hydrostatic model; [b]Plume interpretation; $T = 250$ K is assumed; I = imaging; S = spectroscopy; (t) = tangential.

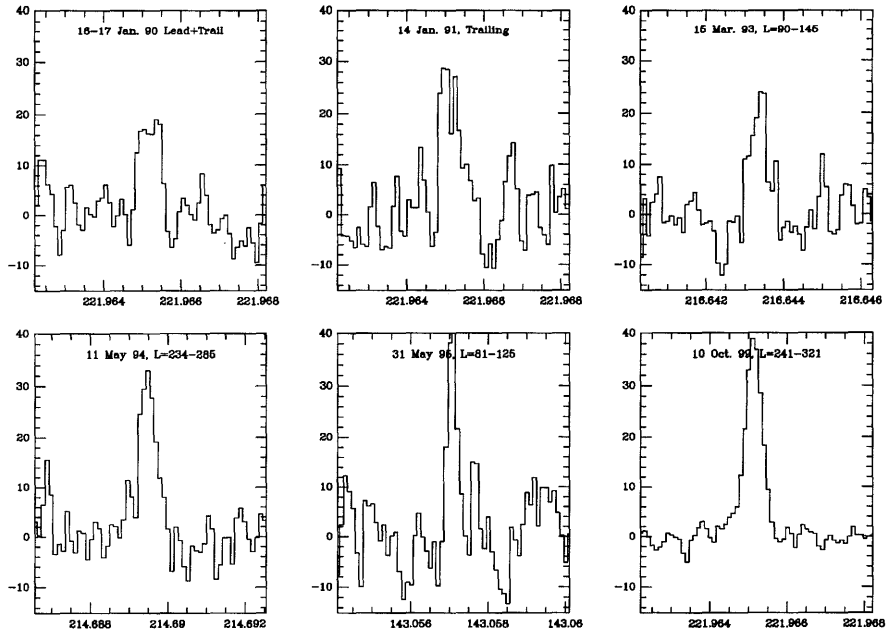

Figure 19.1. Sample millimeter observations of SO_2 emission from Io. The date and Io orbital longitude L are noted for each observation plotted. The plots show brightness temperature contrast (relative to the surface temperature) in degrees K *vs.* frequency in GHz.

16 %, f_h = 6–9 %) for Io's leading atmosphere. For all the observations recorded in 1993 and 1994, the hemispheric-average column is in the range $(1\text{–}2)\times10^{16}\,\mathrm{cm}^{-2}$, with a tendency for higher columns on the trailing side than on the leading. Thanks to an unprecedented signal-to-noise ratio (S/N), the October–November 1999 observations resulted in the detection of many weak lines. Although not yet fully exploited, these observations confirm a cooler and more extended atmosphere on the leading side (Lellouch *et al.* 2000). Best fits of the October 1999 data are obtained for T_{atm} = 200 K and $f_h = 24\,\%$ on the leading, *vs.* $T_{\mathrm{atm}} = 400\,\mathrm{K}$ and $f_h = 8\,\%$ on the trailing. The November 26, 1999 observation constitutes the best data set to constrain the gas temperature, as two close SO_2 lines were detected in the same spectrometer, eliminating possible calibration errors. This indicated $T_{\mathrm{atm}} = 400 \pm 100\,\mathrm{K}$, again on the trailing side. However, the January 2002 observations included the high-energy ($404\,\mathrm{cm}^{-1}$) 265.481 GHz SO_2 line, which indicated a rotational temperature of only 180 ± 60 K (Lellouch *et al.* 2003).

The high temperatures inferred from the millimeter observations on the trailing side using hydrostatic models are at odds with radiative–conductive models (Strobel *et al.* 1994 – see Section 19.2.3) which predict that the atmosphere never warms above 200 K in the first scale height. This may suggest that the hydrostatic interpretation of the millimeter data is incorrect. Ballester *et al.* (1994) first proposed that the millimeter linewidths primarily reflect velocity dispersion within gaseous plumes rather than a combination of temperature and saturation effects. Lellouch (1996) and Lellouch *et al.* (1996, 2000) presented simplified models based on this idea. The hemispheric-average columns of $(0.6\text{–}2.5)\times10^{16}\,\mathrm{cm}^{-2}$ achieved by these models are comparable to those in the hydrostatic models, but the data can now be fit even with low temperatures, and therefore the atmosphere is no longer necessarily "hot and localized". However, because the plumes are small (e.g., r = 135 km for an ejection velocity of ~0.5 $\mathrm{km\,s}^{-1}$ as indicated by the data), they must be very numerous (50–300) to cover a significant fraction of one hemisphere. This large number may be somewhat decreased if allowance is made for a non-zero horizontal flow which increases the plume size. This number can be reduced further if an admixture of small and Pele-class plumes is assumed. With the ~100 active volcanic centers observed by *Galileo* (see Chapter 14 and map of Io in Appendix 1), 50 active plumes may not be unreasonable, especially if many of them are the invisible "stealth" plumes (i.e., those with a low condensate content) postulated by Johnson *et al.* (1995). The possible existence of almost purely gaseous plumes has been demonstrated by Kieffer (1982) in the case of a high-entropy erupting fluid from a reservoir of superheated SO_2 vapor in contact with a deep, hot and dense silicate melt (1400 K, 40 bar). While already complex to implement, the plume models are certainly far from Io's reality, as stressed by Lellouch (1996).

Ultraviolet Observations SO_2 gas absorbs strongly in the UV wavelength region, as shown by the absorption cross section in Figure 19.2. This figure and Table 19.1 summarize the numerous successful UV observations made since the first UV images of Io (Paresce *et al.* 1992) and the first successful UV spectroscopic detection of SO_2 in absorption (Ballester *et al.* 1994). The initial spectroscopic observations (Ballester *et al.* 1994, Clarke *et al.* 1994, Trafton *et al.* 1996) had no spatial resolution and only modest spectral resolution (see Table 19.1). Unlike the millimeter-wave spectrum, the UV observations are primarily sensitive to the column-integrated abundance of the absorbing gas, but

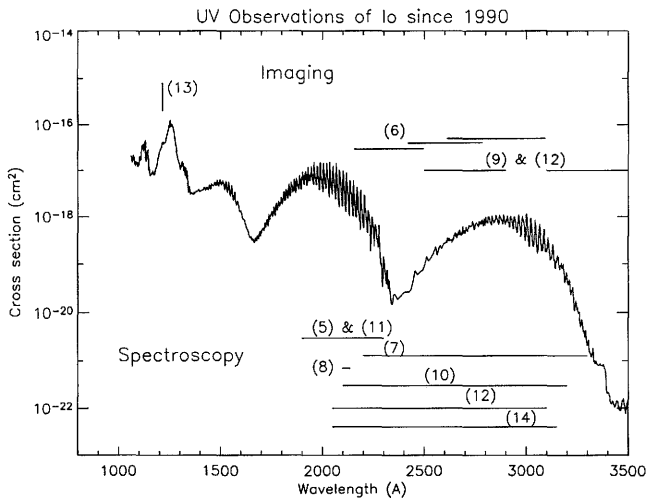

Figure 19.2. SO_2 absorption cross section from Manat and Lane (1993). The numbered horizontal and vertical lines indicate the wavelength coverage of the UV observations summarized in Table 19.1 and discussed in the text.

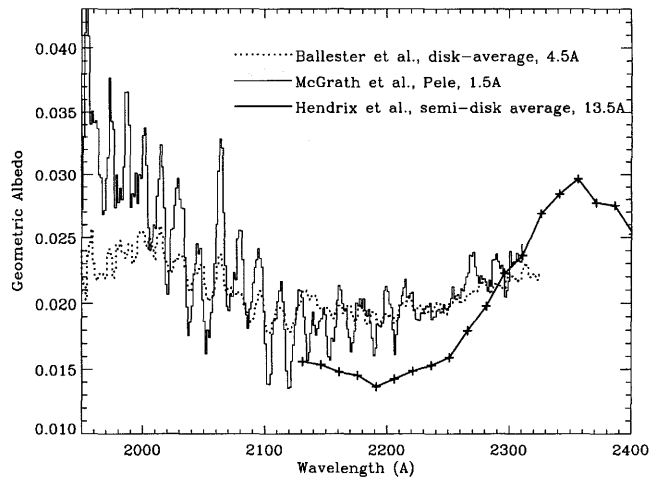

Figure 19.3. Comparison of Ballester *et al.* (1994), Hendrix *et al.* (1999) and McGrath *et al.* (2000a) spectroscopic observations illustrating the importance of spectral resolution in detecting SO_2 in Io's atmosphere.

not to its temperature, except for a general decrease in the band contrast with increasing temperature and subtle variations in the band peak position and skewness (Wu *et al.* 2000). Analysis is subject to two complications, which make unique interpretation of the data difficult. The first comes from the fact that the SO_2 UV spectrum has a very complex structure of many densely packed lines that have not been resolved in laboratory measurements, so that line-by-line position and intensity information is not available. In this situation, applying Beer's law at a spectral resolution comparable to that of the measurements can lead to significant underestimates of absorber abundance (Belton 1982). Band models are much preferred, and several modelers have followed the treatment by Ballester *et al.* (1994) based on a Malkmus intensity distribution of lines with Lorentz profiles and including variations with temperature. The other complication is due to the poorly known contribution of Io's surface to the overall geometric albedo. SO_2 frost, a known constituent of Io's surface, has broadly similar spectral properties as the gas absorption, making the competing optical effects of gas and frost very difficult to disentangle. The reflectance depends sensitively on the frost grain size and how it is physically mixed with the other components. While it is known that SO_2 frost is dark in the UV, it is impossible to reliably predict the absolute surface reflectance and its spectral dependence. As a consequence, only observations with spectral resolution high enough to distinguish characteristic gas spectral features unambiguously constrain gas abundances.

For example, while it is possible to model the early UV imaging data of Sartoretti *et al.* (1994, 1996) purely in terms of variations of surface properties, an alternate explanation is that the darkest UV component seen in the images represents patches of SO_2 gas. In their preferred model, Sartoretti *et al.* (1996) assume that the frost reflectivity is at the lowest value allowed by their data ($R = 0.013$ at 2600 Å), which implies the presence of SO_2 patches with typical columns of $\sim 1 \times 10^{18}\,\mathrm{cm}^{-2}$ covering 11–15 % of the projected surface. One of these patches is Pele, and most others are well correlated with known thermal anomalies (Veeder *et al.* 1994). However, it is important to emphasize that these early UV images were incapable of detecting SO_2 column densities $\lesssim 8 \times 10^{16}\,\mathrm{cm}^{-2}$, so the presence of a more uniformly distributed, lower-density component could not be ascertained.

The lack of spatial resolution in the disk-average spectroscopic observations (e.g., Ballester *et al.* 1994; Clarke *et al.* 1994; Trafton *et al.* 1996), when coupled with the ambiguity in surface reflectance, permits two different model domains to fit the data equally well. The trade-off between spatial coverage and atmospheric column abundance leads to equally good fits with either spatially confined regions with relatively high SO_2 columns, or much more extended coverage with more modest SO_2 column densities. The best fit solutions for both domains are summarized in Table 19.1. The hydrostatic interpretation of the millimeter observations and some of the early UV observations (Trafton *et al.* 1996, Sartoretti *et al.* 1994, 1996) showed a trend to more SO_2 gas on the trailing as opposed to the leading hemisphere.

Another important point for the UV spectroscopy is the lack of detection of SO_2 bands in the near-UV ($\lambda \gtrsim 2500$Å). Clarke *et al.* concluded that this absence of fine structure ruled out a global atmosphere denser than $4 \times 10^{16}\,\mathrm{cm}^{-2}$. However, they pointed out that a very dense, localized component (e.g., $2 \times 10^{19}\,\mathrm{cm}^{-2}$ over 10% area), was not inconsistent with the data. At these very high columns, while structure appears in the region of minimum absorption near 2350 Å, the 2800–3100 Å region is saturated out to 100% absorption, consequently showing no spectral contrast. In addition Hendrix *et al.* (1999) found a clear decrease of the albedo shortward of 2360 Å (see Figure 19.3) which cannot be explained by SO_2 frost. Their interpretation of this decrease as due to SO_2 gas absorption, and not surface reflectance effects, led them to infer very large ($10^{19}\,\mathrm{cm}^{-2}$) SO_2 column densities over at least 25% of the surface.

As both spatial and spectral resolution have improved, spatial variability of the SO_2 atmosphere has begun to be detected directly and quantified. McGrath *et al.* (2000a) obtained spatially resolved spectroscopy at 1.5 Å spectral resolution using a small aperture to target three specific loca-

tions on Io's disk, one of which was Pele. [The importance of spectral resolution adequate to distinguish between gas and frost is illustrated in Figure 19.3, where their data are compared with that of Ballester *et al.* (1994) and Hendrix *et al.* (1999).] The targets were chosen to sample different physical conditions that are likely to exist on Io's surface: (1) the Pele volcano; (2) Ra, a region bright in the visible and dark in the UV, indicating abundant SO_2 frost; and (3) a reference region at 45°S and 300°W ("T3") that is dark in visible and bright in UV, i.e., presumably frost-poor. They derived an SO_2 column density of only $3.25 \times 10^{16} \mathrm{cm}^{-2}$ at Pele (results for the other targets are given in Table 19.1). The observation of T3 was a strong indication of a spatially variable but widespread atmosphere; it is particularly significant to detect SO_2 in a region where no active plume has ever been observed, although this region (Aten Patera) is close to the site of a known hot spot (Lopes-Gautier *et al.* 1999) and seems to have experienced a Pele-like eruption between the two *Voyager* encounters. The analysis of Douté *et al.* (2001) indicates that this region is characterized by low coverage (20–40 %) and fine grain (<150 μm) SO_2 frost.

Spencer *et al.* (1997) imaged the Pele plume against dark sky and silhouetted against Jupiter's disk during Io's transit only 7 days later, showing Pele to be active. Pele's plume height was measured to be 420 ± 40 km, and its opacity at 2720 Å to be ~0.19. The plume was not detected at 3400 and 4100 Å. This wavelength-dependent optical depth was interpreted as due to absorption by either small dust particles (<0.08 μm) with a total mass of at least 1.2×10^9 g, or SO_2 gas with a column abundance of $\sim 3.7 \times 10^{17} \mathrm{cm}^{-2}$. Note that the required mass for SO_2 gas is as much as 100 times larger than for dust, so this interpretation would clearly classify Pele as a "stealth plume." The order of magnitude difference in SO_2 column between the Spencer *et al.* (1997) and McGrath *et al.* (2000a) results was at first thought to be due to particulates accounting for some of the opacity in the UV images. Even so, these SO_2 columns were significantly less than the 10^{18}–$10^{19} \mathrm{cm}^{-2}$ discussed by Sartoretti *et al.* (1994, 1996) and Hendrix *et al.* (1999). When Spencer *et al.* (2000) obtained both imaging and spectrsocopy of the Pele plume again in 1999 they made the spectacular discovery of gaseous S_2 through 15–20 bands belonging to the $B^3\Sigma_u^- - X^3\Sigma_g^-$ system (Figure 19.4), in addition to a detection of SO_2 gas at shorter wavelengths. The S_2 provides a significant source of opacity in the 2500–3000 Å region previously attributed to SO_2. When their tangential SO_2 column density of $\sim 7 \times 10^{16} \mathrm{cm}^{-2}$ is converted to a vertical column (~factor of 2 decrease) it is in remarkably good agreement with the $\sim 3.25 \times 10^{16} \mathrm{cm}^{-2}$ column found by McGrath *et al.* (2000a). In retrospect, the detection of S_2 and SO_2 in the Pele plume at much lower abundance than inferred by Sartoretti *et al.* (1996) and Spencer *et al.* (1997) indicates that the most significant source of opacity in their images may have been due to absorption by gaseous S_2, with negligible dust extinction and only a minor contribution due to gaseous SO_2.

Further evidence in support of the lower density, larger coverage regime has come from HI Lyman-α images of Io obtained by Roesler *et al.* (1999), which has opened a new avenue for studying the distribution of Io's SO_2 atmosphere. Such observations have been acquired in 1997, 1998, 1999, 2000, and 2001, although only the 1997 and 1998 observations have been published to date (Figure 19.5). In the "1998 West" observation (see Figure 19.5) the Lyman-α emission appears to consist of two mid-to-high latitude ($\gtrsim 45°$) bright patches at the 2 kR level, while the equatorial latitudes are dark, with ~0.7 kR at disk center, and longitudinal and/or temporal variations. The brightest Lyman-α emission is entirely within the disk. Although Roesler *et al.* proposed several explanations for the observed structure, differential absorption of surface reflected solar Lyman-α photons by low latitude atmospheric SO_2 was shown to be the most likely by Feldman *et al.* (2000b) and Strobel and Wolven (2001). Since the SO_2 cross section is large at Lyman-α ($\sigma = 3.9 \times 10^{-17} \mathrm{cm}^2$) SO_2 must be a significant absorber for typical SO_2 columns of several $10^{16} \mathrm{cm}^{-2}$. This hypothesis was confirmed by 1999 Lyman-α images taken during and following eclipse. No polar bright regions are apparent in the eclipse images, while they are present in contiguous post-eclipse images, which conclusively links the bright regions near the poles with sunlight.

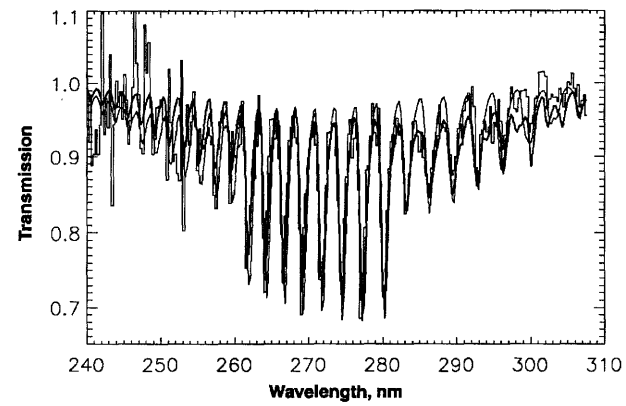

Figure 19.4. Detection of S_2 in the Pele plume by Spencer *et al.* (2000).

The Lyman-α images thus provide a "negative image" of the SO_2 atmosphere, substantially clarifying its spatial structure at scales $\gtrsim 200$ km. Although the problem of disentangling the atmospheric signature from the surface reflecting signature remains, the retrieval of absolute SO_2 columns from these images is facilitated by the fact that SO_2 is a continuum absorber at Lyman-α (enabling the use of Beer's law). Assuming a reflectivity of 0.05 at the poles (which corresponds to a geometric albedo of 0.033), and that the reflectivity is uniform across the disk, Feldman *et al.* (2000b) use Beer's law to determine the optical depth at the sub-Earth point, which corresponds to SO_2 column densities in the range $(1\text{–}4) \times 10^{16} \mathrm{cm}^{-2}$. Strobel and Wolven (2001) constructed a spatial model of the Lyman-α emission for the "1998 West" image shown in Figure 19.5 based on longitudinally homogeneous model atmospheres with column densities decreasing sharply from $(1\text{–}1.7) \times 10^{16} \mathrm{cm}^{-2}$ at the equator to $\sim 3 \times 10^{14} \mathrm{cm}^{-2}$ at 50° and beyond. These models capture the essential observational features and suggest that Io's atmosphere is restricted to an approximately ±30–40° band in which lateral inhomogeneities (at the resolution of the data) are modest. Strobel and Wolven (2001) interpreted this in the context of numerous (10–200) plume atmospheres, with a total vent ejection rate of $\sim 5 \times 10^{30}$ molecules s^{-1}.

Finally, the most recent long-slit UV spectroscopy from HST has achieved the best spatial resolution to date (Jessup *et al.* 2004). The observations cover latitudes from 60° N to 60° S, and include the volcanoes Zamama, Malik, Tupan, and Chaac, as well as SO_2 frost plains. There is only a modest difference in the SO_2 gas column abundance between the Prometheus plume and the nearby low-latitude SO_2 frost plains. Initial analysis shows a smooth transition in SO_2 abundance with latitude, and a fall-off of the abundance at high latitudes, qualitatively consistent with both the Lyman-α imaging and McGrath *et al.* (2000a) results discussed above. Additionally, continuum emission near 2800 Å is observed over the Prometheus plume and neighboring low latitude regions. The continuum emission also appears to correlate with the SO_2 absorption, which peaks at Prometheus. Thus the concept of the SO_2 atmosphere discussed above appears to be more complex than one dominated by scores of active volcanoes. These observations show only modest spatial variability of the SO_2 atmosphere, with relatively small enhancements over active volcanoes, consistent with the McGrath *et al.* (2000a) results.

IR Spectroscopy Ground-based disk-averaged IR observations of Io's atmosphere in November 2001 at a resolution of 50 000 (Spencer *et al.* 2002) resulted in the detection of 15 lines of the ν_2 band of gaseous SO_2 in the 18.9 μm region. The lines appear in absorption, probably due to non-LTE effects that produce absorption even for atmospheric kinetic temperatures somewhat warmer than the surface temperature. Line strength varied strongly with orbital longitude, being greatest on the anti-Jupiter hemisphere. A preliminary analysis of the data gives disk-averaged SO_2 column densities of $\sim 2 \times 10^{16}$ and $1 \times 10^{17}\,\mathrm{cm}^{-2}$ at $L = 16°$ and 213° respectively. They also attempted to detect the SO_2 ν_3 band at 7.3 μm seen by Pearl *et al.* (1979) over Loki. A 15-minute integration showed no absorption at sensitivity levels that should have detected the absorption strength seen by Pearl *et al.* (1979).

Minor Compounds

Beyond SO_2, a number of other compounds have been searched for in Io's atmosphere. SO was first clearly detected in 1995 millimeter observations at 219.949 and 138.176 GHz on both sides of Io (Lellouch *et al.* 1996), and confirmed in 1999 at 251.825 and 109.252 GHz. The strongest SO lines appear typically two times weaker than the strongest SO_2 lines, although they are intrinsically five to ten times more intense, implying that SO is a minor compound. In the framework of hydrostatic models the observations cannot distinguish between a hemispheric SO atmosphere – in this situation, a barely collisionally thick SO atmosphere with a $(2\text{–}6)\times 10^{14}\,\mathrm{cm}^{-2}$ column is indicated – and an SO component colocated with SO_2 on a restricted fraction of Io's surface with a 4–10 % SO/SO_2 mixing ratio. In the case of volcanic models, the SO/SO_2 mixing ratio within the erupting plumes is also in the range 3–10%. The McGrath *et al.* (2000a) data also show several weak features consistent with SO bands that give a relative mixing ratio to SO_2 of about 10%, consistent with the millimeter-wave detections.

Another important measurement of SO was made using infrared spectroscopy of Io during eclipse in 1999, which led to the detection of the forbidden electronic $a^1\Delta \rightarrow X^3\Sigma^-$ transition of SO at 1.71 μm (de Pater *et al.* 2002). The detection was later confirmed by Goguen and Blaney (2001). These emissions are attributed to gas from the volcanic vents Loki and Janus/Kanehekili for the two observations, respectively. The de Pater *et al.* (2002) observations indicate an emission rate of $\sim 2 \times 10^{27}$ photons s^{-1}. They discussed many possible mechanisms for this emission and concluded it to be caused by direct ejection of SO molecules in the excited $a^1\Delta$ state from the vent at a quenching temperature of $\sim$ 1500 K. The shape of the band indicates a rotational temperature of $\sim$ 1000 K. Because rotational levels are easily thermalized, this temperature may represent the actual kinetic temperature of the emitting gas as it is vented.

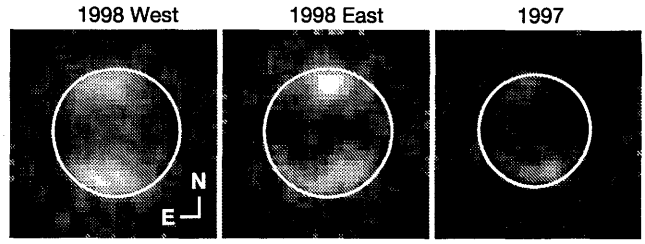

Figure 19.5. Monochromatic images of Io in HI Lyman-α (1216 Å). Bright regions show areas where solar Lyman-α is reflected from the surface, largely unattenuated by SO_2 gas; dark areas correspond to more SO_2 gas absorption.

As mentioned above, Spencer *et al.* (2000) discovered S_2 in the Pele plume (see Figure 19.4). Best fit models indicate an S_2 (tangential) column density of $(1 \pm 0.2)\times 10^{16}\,\mathrm{cm}^{-2}$ and a temperature of 300 K. Since SO_2 is detected in the same observation, an SO_2/S_2 ratio of $\sim$3–12 can be inferred. The discovery of S_2 was not unexpected, since sulfur vapor had been proposed to be the driver of the Pele plume (McEwen *et al.* 1988), but the apparent dominance of SO_2 gas was not predicted. Given the observed abundances, the equivalent resurfacing rates by SO_2 and S_2 are 0.12 and 0.8 $\mathrm{mm\,yr}^{-1}$ in the Pele plume deposits. The S_2 detection may be the key in explaining the red deposits near Pele and other active regions, as S_2 is unstable against photolysis, producing reddish S_3 and S_4 molecules by polymerization. However, S_2 also reacts rapidly with O atoms ($k = 2.2 \times 10^{-11}\, e^{84/T}\,\mathrm{cm}^3\,\mathrm{s}^{-1}$) and S reacts rapidly with O_2 ($k = 2.2 \times 10^{-12}\,\mathrm{cm}^3\,\mathrm{s}^{-1}$). To polymerize to S_3 and S_4 would require an environment with a low total O to total S ratio such as in the vicinity of Pele.

The first detection of gaseous NaCl was achieved in January 2002 (Lellouch *et al.* 2003) via the detection of emission lines at 234.252 and 143.237 GHz. The disk-averaged column density is in the range $(0.8\text{–}20)\times 10^{13}\,\mathrm{cm}^{-2}$, with a preferred value of $4 \times 10^{13}\,\mathrm{cm}^{-2}$, i.e., about 0.4% of SO_2. Because of its vanishingly low vapor pressure at Io's temperature, the most likely source of NaCl is direct volcanic output, although sputtering of salt-bearing atmospheric aerosols is not excluded. Volcanic plume models indicate total volcanic emission rates of $(2\text{–}8) \times 10^{28}$ NaCl molecules s^{-1}, i.e., typically 0.3–1.3% of the SO_2 rates. NaCl is probably restricted to smaller regions than SO_2 because of increased photolytic and condensation losses.

Eight other compounds (CO, H_2S, OCS, S_2O, ClO, CS,

NaOH, KCl) have been searched for unsuccessfully at millimeter wavelengths. The most significant of the associated upper limits is probably the stringent 10^{-10} bar upper limit on a global H_2S atmosphere (Lellouch *et al.* 1992). An upper limit of $2 \times 10^{14}\,\mathrm{cm}^{-2}$ was set for the abundance of CS_2 by McGrath *et al.* (2000a).

Atomic Species

Five atomic species have been detected in emission to date in Io's atmosphere: O, S, Na, K, and Cl. O, S, and Cl are detected via collisional excitation of neutrals in the atmosphere and corona by plasma torus electrons, while Na and K are observed primarily via their strong resonant fluorescence transitions at visible wavelengths. Atomic sulfur and oxygen have been observed extensively both far from Io in the plasma torus since 1981 (Brown 1981, Durrance *et al.* 1983), and near Io since 1986 (Ballester *et al.* 1987). A current unresolved issue is whether the predominant mechanism for the collisionally excited emissions near Io is direct excitation of atomic species, or dissociative excitation of molecular species. Observations of these emissions are not straightforward to interpret as regards atmospheric properties because they represent an integrated brightness along the line of sight that is a product of the electron and neutral densities and the appropriate rate coefficient, itself a function of electron temperature. The integrated brightness is therefore diagnostic of both the plasma conditions and the relevant neutral densities, and information about the two are difficult to disentangle unambiguously. A common approach used to estimate neutral column densities is to assume that the excitation process is electron impact of atomic species, and that both the electron density and temperature are constant along the line of sight, both of which are poor approximations. The plasma properties near Io are complex (Linker *et al.* 1998, Combi *et al.* 1998, Saur *et al.* 1999), and currently forward modeling, as opposed to inversion, is more successful at deriving information about the atmosphere (cf. Saur *et al.* 2000). Interpretation is also complicated by variations due to observing geometry and the location of Io relative to the plasma torus equator. Finally, especially for atomic sulfur, there is very limited information available about the relevant rate coefficients. Hence although there are extensive observations of the atomic emissions, such as those of Oliversen *et al.* (2001), relatively little information about atmospheric properties has been extracted from them. We provide here a brief summary of the atmospheric diagnostics; the derived plasma properties are described in more detail in Chapter 22.

Electron temperature and column density estimates for O and S were first made by Ballester (1989) using disk-average International Ultraviolet Explorer (IUE) spectra. The oxygen emissions were found to be consistent with the excitation of oxygen in Io's exosphere by nominal $\sim$5 eV torus electrons. Minimum oxygen column densities of $\mathcal{N}_O > (4\text{–}7)\times10^{13}\,\mathrm{cm}^{-2}$ were required to produce the emissions assuming canonical torus values of $T_e = 5\,\mathrm{eV}$ and $n_e = 2000\,\mathrm{cm}^{-3}$. Employing information about the optical depths of the allowed and forbidden transitions of atomic sulfur, Ballester (1989) also derived limits on the sulfur column density of $2.2 \times 10^{12}\,\mathrm{cm}^{-2} < \mathcal{N}_S < 7 \times 10^{15}\,\mathrm{cm}^{-2}$. In the spatially resolved spectroscopic observations of McGrath *et al.* (2000a) described earlier, emission from the SI] 1900,1914 Å doublet was detected in two of their three targets, with intensities of 3.6 kR over Pele and 1.6 kR over T3. The sulfur column above Pele was estimated to be $\mathcal{N}_S \sim 1 \times 10^{14}\,\mathrm{cm}^{-2}$ using techniques similar to Ballester (1989). Using HST/STIS data, Feaga *et al.* (2002) were able to resolve the optically thick allowed and optically thin forbidden sulfur transitions at 1479 Å, which provided a significantly improved estimate of the tangential sulfur column density of $3.6 \times 10^{12}\,\mathrm{cm}^{-2} < \mathcal{N}_S < 1.7 \times 10^{13}\,\mathrm{cm}^{-2}$ that is independent of electron density and temperature. [Using more recent atomic data for sulfur has now raised this upper limit to $1.3 \times 10^{14}\,\mathrm{cm}^{-2}$.] Using the 1-D photochemical model of Summers and Strobel (1996), and assuming spherical symmetry, the vertical column density would be about a factor of 7 lower.

The observations that produced the Lyman-α images discussed above have also provided simultaneous monochromatic images of the far-UV S and O emissions. Along with *Galileo* broadband SSI images (Geissler *et al.* 1999) these data have revealed the complex morphology of the emissions, which is characterized by five notable features: equatorial "spots", volcanic plume glows, a limb-brightened ring of emission just off the disk, diffuse atmospheric emissions (also referred to as "glow"), and emission from Io's extended corona. The spots (often referred to as the "Io aurora") are observed to rock about the equator in concert with the changing orientation of the background jovian magnetic field, which provides a powerful tool to infer properties of the strong electrodynamic interaction between plasma and satellite. The limb-brightened rings of sulfur and oxygen emission imply that both species form global components of the atmosphere.

The *Galileo* SSI images of Io (Geissler *et al.* 1999) were acquired over the course of 14 eclipses from 1996–1998. While most of the observations were made using the SSI clear filter (wavelength coverage of 3800–10 400 Å), several sequences included imaging with the violet (3800–4450 Å), green (5100–6050 Å) and red (6150–7100 Å) filters. The equatorial spots were seen with all of the filters, but were brightest in the violet filter images. The diffuse atmospheric glow was seen against the disk of Io in the green filter, and particularly on the nightside in the E15 orbit observations. The identity of the emitters could not be unambiguously determined because of the broad wavelength coverage of the filters, however, several candidates were proposed by Geissler *et al.* (1999), including [OI] 6300 and 6360 Å, Hα 6560 Å, and SII 6720,6730 Å in the red filter; [OI] 5580 Å and NaI 5890,5900 Å in the green filter; and molecular emission from SO_2 in the violet filter. High resolution Keck spectra obtained by Bouchez *et al.* (2000) detected auroral emission from [OI] 6300,6363,5577 Å, and Na 5889,5896 Å. They concluded that the red filter emissions seen by *Galileo* SSI were from the oxygen lines, and the green emissions were from the Na lines. They detected no emissions in the SSI violet region, lending support to the idea that the *Galileo* violet emissions are from broadband continuum emission from SO_2 or SO.

HST/STIS observations have provided the first simultaneous spatially resolved measurements of emission from sulfur and oxygen. Wolven *et al.* (2001) used them to derive spatial profiles of the sulfur and oxygen emissions with a

spatial resolution of $\sim 0.05\,R_{Io}$ out to distances of $\sim 10\,R_{Io}$. The coronal emission profiles vary considerably in slope and intensity, and are generally brighter when Io is on the dusk side of Jupiter. The intensities of emission from regions both near Io and in the extended corona vary with System III longitude in a near-simultaneous fashion, suggesting torus electron density as the probable source of this modulation. The observed ratio of oxygen to sulfur emission is relatively constant in time, perhaps reflecting the stoichiometric ratio of the SO_2 source molecules. A dramatic increase in profile emission brightness and slope between eclipse and post-eclipse observations in February 2000 suggests a dynamic response by a sublimation-supported component of Io's SO_2 atmosphere and associated atomic species.

It has long been believed that Io's SO_2 atmosphere condenses on to the surface when Io goes into eclipse. Several observations bear on this question. Visible emissions were seen during eclipse by *Voyager 1* and were thought to be from SO_2 (Cook *et al.* 1981). Disk-averaged observations of Io passing into Jupiter shadow acquired by Clarke *et al.* (1994) showed that the far-UV sulfur and oxygen emissions, which had typical brightnesses of 1 kR when Io was in sunlight, decreased to only a few hundred Rayleighs within 20 min of Io entering eclipse. Geissler *et al.* (1999) report on the changes seen in a set of two SSI images obtained 11 min after the start of eclipse and 41 min later in orbit E15. Io's disk clearly darkened as the eclipse progressed, while a difference image shows that the plume glows have brightened (see their Fig. 2). Wolven *et al.* (2001) report on HST/STIS observations obtained on February 25, 2000 which show a dramatic increase in S and O brightnesses after eclipse egress. Retherford (2002) quantified these changes for the spots, the limb glow, and the extended corona. A thorough discussion of the timescales of various changes in the atmosphere (both atomic and molecular) associated with eclipse ingress and egress is presented by Retherford (2002; see his Chapter 5, especially Table 5.2). He concludes that after ingress, the sublimation atmosphere will collapse on a timescale of $\sim$5 min, followed by a depletion of the atomic atmosphere within (conservatively) $\lesssim$30 min. The atomic corona, however, is depleted on a timescale of $\sim$280 min, which is longer than the duration of an eclipse ($\sim$130 min), consistent with the STIS eclipse observations.

Cl has been detected with HST (Retherford *et al.* 2000, Feaga *et al.* 2004), however, the lack of adequate S/N and reliable electron excitation rate coefficients have hindered interpretation of the data, and only poorly constrained estimates of the abundance are available. Preliminary analysis indicates that Cl may be present in amounts comparable to that of Na (Feaga *et al.* 2004).

Because they have very large oscillator strengths and are therefore easily detected even at very low densities, observations of visible wavelength resonance fluorescence lines of sodium and potassium have been very important in studies of Io's atmosphere. In fact, much of what we know about the atmospheric dynamics and Io's interaction with the plasma torus comes from sodium observations. Mutual eclipses between Io and other Galilean satellites (Schneider *et al.* 1991, Burger *et al.* 2001) have allowed observations of Io's corona inside the Hill sphere ($\sim 5.8\,R_{Io}$), down to $\sim 1.4\,R_{Io}$, from which radial profiles of Na column density have been derived. Burger *et al.* (2001) have also shown that the Na corona is denser on the sub-Jupiter compared to the anti-Jupiter side, with the average radial profile $\mathcal{N}_{Na}(b) = 2.2 \times 12\,b^{-2.34}$ for $b > 1.5\,R_{Io}$. Bouchez *et al.* (2000) eclipse spectroscopy detected Na emission, most likely excited by torus electrons, from which they derived a disk-average column density (assuming nominal torus conditions) of $\mathcal{N} \sim 4 \times 10^{12}\,\mathrm{cm}^{-2}$, which is comparable to the Na column density derived by extrapolating the Schneider *et al.* (1991) and Burger *et al.* (2001) profiles to the surface. Potassium measurements have only been made down to $\sim 10\,R_{Io}$ due to the weaker emission intensity, giving column densities at that distance of $\sim(0.4\text{–}1.5) \times 10^9\,\mathrm{cm}^{-2}$. Contemporaneous measurements of Na allow the Na/K ratio to be derived, and it is approximately constant from $\sim$10–20 R_{Io} at a value of 10 ± 5 (Brown 2001).

The source of alkalis to Io's atmosphere is still not certain, in part because the observations are principally of escaped sodium in extended clouds rather than in the bound atmosphere near the surface. The salty satellite models (Fanale *et al.* 1974, Kargel 1991, Zolotov and Shock 2001) suggest that sodium might occur as a sulfate. The presence of Cl in amounts comparable to Na may imply that the initial volcanic source contains NaCl, although Cl could occur in other molecular forms (Zolotov and Shock 2001). The recent detection of NaCl indicates that this gas is a quantitatively plausible source of sodium and alkalis in Io's atmosphere. Since NaCl from a volcanic source efficiently dissociates, the resulting Na and Cl would react separately with the principal surface constituents, frozen SO_2 and its radiation products. Chlorine was therefore suggested to be present on the surface as Cl_2SO_2 (Schmitt *et al.* 2001) and Na as Na_2SO_4 (Wiens *et al.* 1997) or Na_2S_x (Chrisey *et al.* 1988).

The vapor pressure of likely sodium-bearing molecules is low at the ambient surface temperatures on Io, leading Matson *et al.* (1974) to suggest initially that the source of the observed sodium was sputtering by the plasma trapped in Jupiter's magnetosphere. The corotating plasma ions do not reach Io's surface due to its ionosphere and collisionally thick SO_2 atmosphere. However, estimates of the energetic ion flux that does reach the surface suggest it could provide an adequate source of surface sputtered sodium (Wong and Johnson 1996b). An alternate source is direct population of the atmosphere from vents and volcanic plumes. Laboratory studies show that energetic ions, as well as photons and electrons (Wiens *et al.* 1997, Chrisey *et al.* 1988, Madey *et al.* 1998), preferentially remove alkalis from refractory materials by an electronic sputtering process that also causes decomposition of such materials. The sodium ejected in this fashion is predominantly atomic, with a smaller fraction in molecular form. The discovery that a component of the torus is sodium-containing molecular ions (Wilson and Schneider 1994) led to estimates of the abundance of molecular Na at the exobase. Unlike SO_2, Na is mostly in atomic form near the exobase (see, e.g., Wong and Johnson 1995). The molecular ions are then supplied to the torus by ion–molecule reactions near the exobase (Johnson 1994), or by direct flow along field lines that connect with the ionosphere (Wilson and Schneider 1999, Wilson *et al.* 2003).

Sodium emission has also been seen far up and down stream from Io. In addition, a giant nebula of escaping sodium (referred to as the jovian xeno-corona) has been seen

out to ~500 jovian radii (Mendillo *et al.* 1990). These Na observations clearly indicate that Io's atmosphere is escaping and the ejected material supplies the Io torus. They have been used to derive a detailed description of atmospheric loss (Smyth and Combi 1997, Wilson *et al.* 2003). This is discussed in more detail in Chapter 23. Smyth and co-workers (Smyth and Marconi 2000) have applied the ideas learned from escape of sodium to loss of the principal species from Io's atmosphere.

Ionosphere

Only two sets of detections of Io's ionosphere have been made in the past 30 years, the first by the *Pioneer 10* spacecraft, and the second by the *Galileo* spacecraft. A useful summary of the *Pioneer 10* observations and their interpretation, which met with only limited success, is given by Johnson and Matson (1989). It is important to emphasize that the nature of the radio occultation measurements results in a viewing geometry that always puts both the entrance and exit measurements within a few degrees of the terminator. As a result, both the entrance and exit measurements primarily sample the sunlit atmosphere – even when they occur above the nighttime terminator, only the lower few km of the atmosphere is in darkness.

Results from a series of six *Galileo* radio occultation measurements in 1997, published in a single comprehensive paper by Hinson *et al.* (1998), have greatly clarified the situation with Io's ionosphere. These occultations sampled a wide variety of geometries of the sunlit hemisphere relative to the plasma ram direction. The measurements yield information about the distribution and motion of the plasma near Io. The distribution was found to have two components. The first is present within a few hundred km of Io's surface throughout the upstream and downstream hemispheres and resembles a bound ionosphere. Vertical electron density profiles for this component were derived at 10 locations near Io's terminator. The peak density exceeded $5 \times 10^4\,\mathrm{cm}^{-3}$ at 9 out of 10 locations, and reached a maximum of $2.8 \times 10^5\,\mathrm{cm}^{-3}$. The peak density varied systematically with Io longitude, with maxima near the centers of the sub- and anti-jovian hemispheres, and minima near the centers of the downstream and upstream hemispheres. This pattern may be related to the Alfvénic current system induced by Io's motion through the magnetospheric plasma (see Chapter 22). The vertical extent of the bound ionosphere increases from ~200 km near the center of the upstream hemisphere to ~400 km near the boundary between leading and trailing hemispheres.

The second component is highly asymmetric, consisting of a wake or tail that appears only on the downstream side and extends to distances as large as 10 Io radii. Plasma near Io's equatorial plane is moving away from Io in the downstream direction, with velocity increasing from 30 to $57\,\mathrm{km\,s}^{-1}$ between 3 and 7 Io radii. The latter velocity corresponds to corotation, suggesting that bulk plasma motion, rather than wave motion, was being observed. It is apparent that the major factor determining the morphology of the ionosphere is the plasma ram direction. The *Galileo* measurements generally confirm the original *Pioneer 10* results, providing strong evidence, given the 23 year time span between measurements, that the ionosphere is stable. Most modeling of Io's ionosphere to date has attempted to match the *Pioneer 10* entrance profile, which is now clearly understood from *Galileo* measurements to be dominated by electrons on the flanks. The inability of the one-dimensional photochemical models to match this profile is therefore understandable.

Variability

Several sets of data show that Io's atmosphere exhibits a relatively large degree of stability in a global sense: those of the ionosphere from *Pioneer 10* and *Galileo*; the long-term Na observations (Schneider *et al.* 1991, Burger *et al.* 2001); and the permanent detectability of the SO_2 atmosphere. Nonetheless, several independent lines of evidence from the observations discussed above also suggest significant temporal variability of the atmosphere. The non-detection of IR absorption from the Loki region by Spencer *et al.* (2002) described above may indicate significant variability compared to the *Voyager* epoch, although a different interpretation is not precluded because of the lack of spatial resolution in the more recent observations. In some of the Lyman-α images the north polar bright region is almost absent, and several images covering approximately the same longitudes but at different times (cf. the 1997 image in Figure 19.5 is also "West" and can be qualitatively compared with the 1998 West image – see also Table 19.1 in Feldman *et al.* 2000a) show changes in the brightness and extent of the polar spots, indicating a greater or lesser latitudinal extent of the SO_2 atmosphere. The Strobel and Wolven (2001) analysis of the August 1998 Lyman-α image derived a low latitude column of $\sim(1\text{–}2) \times 10^{16}\,\mathrm{cm}^{-2}$, in good agreement with the McGrath *et al.* (2000a) spectroscopic result for Pele and Ra at similar latitude, but a column of $\sim 3 \times 10^{14}\,\mathrm{cm}^{-2}$ for latitude $\gtrsim 45°$ compared to the McGrath *et al.* (2000a) value of $7 \times 10^{15}\,\mathrm{cm}^{-2}$ at a latitude of 45° S, which is more than an order of magnitude larger. This would be consistent with the observed differences in the Lyman-α images mentioned above. Significant changes over relatively short time periods have also been seen in the Lyman-α images (e.g., October 1999), however, it is unclear if these changes are temporal or spatial, as the central longitude of Io also changed significantly during the course of the observation.

While the SO_2 millimeter emissions appear to be permanently detectable, this ensemble of data also provides evidence for temporal variability. In June 1995, the trailing side 143.057 GHz line appeared sharper and narrower than in previous years (see Fig. 8 of Lellouch 1996). In the framework of the hydrostatic equilibrium models, this suggests a reduction of either the column density or the temperature, and an increase in the areal extent. In fact, this observation, unlike all others, is consistent with a hemispheric atmosphere. In October 1999, the 221.965 GHz line was about 50 % stronger than in 1990–1994, interpreted as a generally higher surface coverage. Beyond the leading/trailing differences discussed above, the 1999 observations allowed, for the first time, to search for orbital variations of strong line characteristics. While no obvious variability of the linewidth was found, there is a suggestion of an increase of the line area over $L = 40 - 135°$ and a decrease over $L = 240 - 340°$ (Figure 19.6a), consistent with the Spencer *et al.* (2002) 19 μm data. More definite is the variation of line frequency with

orbital position, with a global blueshift by $\sim 100\,\mathrm{m\,s^{-1}}$ on the leading side and a similar redshift on the trailing side (Figure 19.6b). The 1993–1995 data are also consistent with this behaviour. In the plume models described above, gas particles flow towards the observer near plume center, and away from the observer near plume edges. Because of saturation near plume center, these models produce slightly asymmetric and redshifted (100–$200\,\mathrm{m\,s^{-1}}$) lines. This is consistent with the trailing side observations, but opposite to the leading side results. The interpretation might be related to angular momentum transfer from the plasma flow hitting Io's trailing side at $\sim 57\,\mathrm{km\,s^{-1}}$. Saur *et al.* (2002) present evidence for torus ion drag forces compressing the ram/upstream atmosphere and extending the downstream atmosphere with a respective scale height ratio of 1/2. The ion drag forces will set the neutral gas in motion to yield a global blueshift on the leading/downstream side and a global redshift on the trailing/upstream side. We note that this type of gas motion has been deduced from the *Galileo* radio occultation measurements, which were described above.

Two additional pieces of evidence support the idea of temporal variability. A second set of Jupiter transit observations of Pele in 2003 do not show a strong S_2 signature, as contrasted with the 1997 detection described above (Spencer *et al.* 1997), indicating temporal variability in plume gas abundance and/or composition. Finally, during a 6-month monitoring campaign in 1991–1992 Brown and Bouchez (1997) saw a large change in the Na emission intensity in the extended cloud, which they inferred was caused by a volcanic outburst, followed a short time later by an increase in torus S^+ emission intensity, which they attributed to an increase in mass loading of the torus.

19.2.3 Recent Progress: Modeling

Although observations have begun to elucidate the nature of Io's atmosphere, they are still relatively infrequent and many gaps remain in our knowledge. Theoretical models provide complementary details that allow us to gain a more complete picture. Because comprehensive, self-consistent models are very difficult to construct, most attempts at modeling Io's atmosphere have focused on single aspects of the problem, namely vertical composition and density structure (Kumar 1982, Kumar and Hunten 1982, Kumar 1985, Summers 1985) or the horizontal distribution of surface pressure and its associated dynamics (Fanale *et al.* 1982, Matson and Nash 1983, Ingersoll *et al.* 1985, Ingersoll 1989, Moreno *et al.* 1991). Even though these simplified models had only moderate success in reproducing the *Pioneer 10* ionospheric density profiles, they did indicate that Io's atmosphere must contain significant amounts of SO, O_2, O and S. But the progress made in the last decade has now justified the development of more elaborate, two-dimensional models. We discuss here the latest efforts in the "single aspect" models, as well as the first attempts at "unified" models.

Modern Buffered Model

The early UV observations of Ballester *et al.* (1994) motivated Kerton *et al.* (1996) to reconsider the radiative equilibrium models of Fanale *et al.* (1982) because they gave SO_2 abundances larger than observed. They rectified some of the oversimplifications in the treatment of radiative equilibrium by taking into account the latent heat of SO_2 frost sublimation, the rotation rate of Io, thermal conduction and Io's internal heat flow, and the deposition of some solar energy below the surface (a component of the so called "icy greenhouse" effect). Accounting for heat conduction shifts the maximum temperature slightly from the subsolar point toward the dusk terminator. The surface temperature and pressure gradients toward the periphery of Io's disk are much more gradual than for the radiative equilibrium case. These enhancements to the model resulted in reduced column abundances more consistent with the Ballester *et al.* (1994) results. An essential point is that these models don't assume a surface temperature dependence (and hence SO_2 sublimation source) that is axisymmetric about the subsolar point. In the most extreme cases (the high conductivity C/R/L – thermal conduction, rotation, latent heat – model, their Figure 6, and the subsurface greenhouse model, their Figure 8) the SO_2 pressure near the poles is many orders of magnitude lower than near the terminators, which is qualitatively consistent with interpretations of the Lyman-α images (Feldman *et al.* 2000b, Strobel and Wolven 2001).

Volcanic Models

The more detailed plume composition information now available from the Spencer *et al.* (2000) and McGrath *et al.* (2000a) observations has enabled detailed thermochemical modeling of volcanic eruptions on Io. A series of papers by Zolotov and Fegley (Zolotov and Fegley 1998a,b, 1999, 2000, Fegley and Zolotov 2000) has presented results of ideal gas thermochemical equilibrium calculations to evaluate volcanic gas chemistry. Since some of the hot spot temperatures on Io range up to 1700 K, they argue that, by analogy with volcanic eruptions on Earth where volcanic gases erupted at temperatures $\geqslant 900$ K are high enough for thermochemical equilibrium, ionian gases may also chemically equilibrate during eruptions. They substantiated this by comparing the eruption times to the chemical lifetimes for volcanic gas chemistry. The eruption temperature, total pressure and bulk elemental composition of the volcanic gases are inputs to the modeling, and thermochemical equilibrium inside the volcano, and quenching in the vicinity of the volcanic vent are assumed. The composition of the erupted gas is then used to evaluate magma temperature and the oxidation state of the magma and Io's interior, to infer thermal and chemical conditions in the volcanic source region, and to calculate pressures in the vicinity of the vent. The earlier papers used compositional information from the Io plasma torus due to the lack of quantitative information about the plumes or atmosphere of Io. These models imply that the Pele plume gas last equilibrated at magmatic temperature and was not significantly altered in the eruption. The composition of the Pele plume indicates that Io is differentiated, and that metallic iron and free carbon are not abundant in bulk silicate on Io. Zolotov and Fegley (1998a) stress that SO is a natural product of thermodynamical equilibrium in erupted materials, and that the observed SO/SO_2 mixing ratio can be fit for suitable combinations of gas pressure, temperature and a value of $O/S < 2$ at the vent. They also predict S_2O to be an important volcanic species. Also of

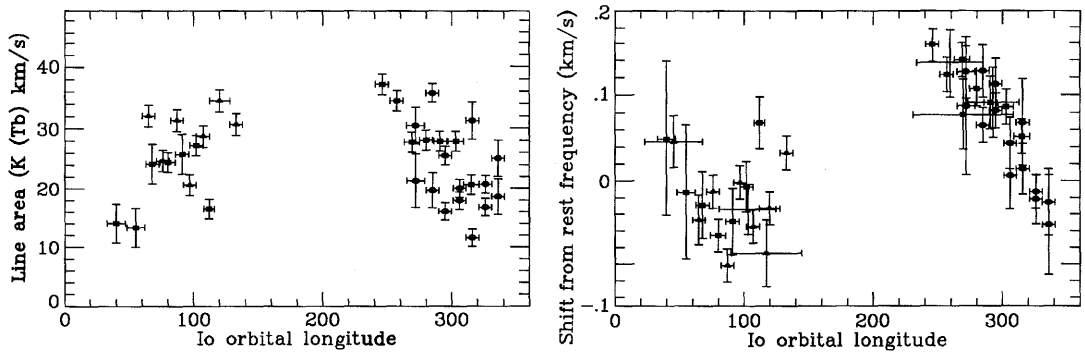

Figure 19.6. The SO_2 mm emission line area (left) and shift from rest frequency (right), which illustrate the variability of the SO_2 atmosphere discussed in the text.

note is the detailed modeling of the temperature structure of volcanic plumes recently achieved by Zhang *et al.* (2003).

Radiative and Photochemical Models

The radiative and photochemical models described in this section involve one-dimensional calculations in which only the vertical thermal or density structure is modeled. In all cases the SO_2 density profile is assumed to be in hydrostatic equilibrium and not affected by photochemical and transport processes.

Strobel *et al.* (1994) developed the first comprehensive model of Io's vertical thermal structure, extending and improving on the treatments by Kumar (1985) and Lellouch *et al.* (1992). They solved the time-dependent, one-dimensional heat balance equation with heat transport by diffusive and radiative processes, including solar heating in the UV and a detailed description of non-LTE cooling by SO_2 rotational and vibrational lines. Two cases were considered, a high-density atmosphere representative of the [smaller fractional coverage, higher column abundance] regime typified by the millimeter observations, and a low-density atmosphere intended to represent the [larger fractional coverage, lower column abundance] regime typified by the early disk-averaged UV observations. Their model predicts the existence of a mesopause in Io's atmosphere when the surface pressure exceeds ~10 nbar. None of the model atmospheres generated with only solar heating were hot enough to satisfy the hydrostatic interpretation of the millimeter data, or the bulk atmospheric temperature of 200–400 K derived from the UV data because the relevant temperature is the average temperature (~140 K) of the first scale height (~10 km). Two additional sources of heating were therefore explored: the heating associated with impacting thermal ions from the Io plasma torus as they sweep by Io's exosphere/upper atmosphere (Johnson and Matson 1989), and Joule heating, which is driven by the penetration of Jupiter's corotational electric field into Io's conducting ionosphere (see Figure 19.7). In agreement with the earlier results of Lellouch *et al.* (1992) they found that unless the plasma penetrates significantly below the exobase it would only elevate the exospheric temperature. In the limit of atmospheres with surface pressures in the range 0.1–1 nbar, Joule heating can in principle produce a warm atmosphere with average temperature greater than 200 K.

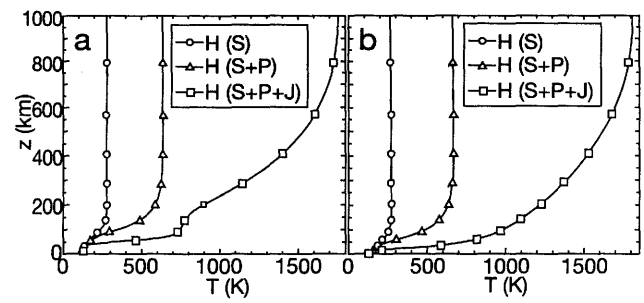

Figure 19.7. The effects of solar (S), solar + plasma (S+P) and solar + plasma + Joule (S+P+J) heating (H) on the thermal structure of Io's atmosphere (Figure 12 from Strobel *et al.* 1994). Panel a: $T = 130$ K and $P = 130$ nbar; panel b: $T = 120$ K and $P = 3.5$ nbar at the surface.

Making use of the thermal structure of Strobel *et al.* (1994), Summers and Strobel (1996) focused renewed effort on the photochemical modeling in order to gauge the sensitivity of the chemical structure to vertical transport rates, and to evaluate the possibility that O_2 and/or SO may be significant dayside constituents. Unlike the earlier photochemical models, they tested both low and high values of the eddy mixing rate. Minor molecular Na species were included in the calculations. The molecular and atomic Na escape rates of Wilson and Schneider (1994) and Smyth and Combi (1988), respectively, were used as constraints in the modeling, and they attempted to match the *Pioneer 10* dayside ionospheric profile. Their results confirmed the prediction (Kumar 1985) that SO is an important atmospheric constituent. None of the cases considered could simultaneously both produce the large atomic and molecular Na escape rates, and provide a reasonable match to the *Pioneer 10* ionospheric profile. They concluded that SO_2 photochemistry alone could not produce the O_2 column abundance suggested by Kumar and Hunten (1982), but that SO could potentially become a dominant background gas globally since it might not condense during Io night.

Moses *et al.* (2002a,b) have revisited the one dimensional aeronomic models in order to address how active volcanism might affect the standard picture of photochemistry on Io. A variety of sodium, potassium, and chlorine-bearing volatiles are included, in addition to sulfur and oxygen species. Unlike the previous models, they assume that a Pele-type volcanic source continuously supplies gas at the

surface. The Zolotov and Fegley type thermochemical equilibrium calculations described above are used to help constrain the composition and physical properties of the exsolved volcanic gases. The effects of photolysis, chemical kinetics, condensation, and vertical eddy and molecular diffusion are then tracked to determine the subsequent evolution of the gas. Moses *et al.* (2002a) focuses on sulfur and oxygen species. As might be expected, if S_2 is a common volcanic gas, the sulfur species (S, S_2, S_3, S_4, SO, and S_2O) are enhanced relative to the oxygen species (O and O_2) in their Pele-type volcanic models as compared with frost sublimation models. The indication of a higher SO/SO_2 ratio in the Pele plume (McGrath *et al.* 2000a) may reflect the importance of volcanic SO rather than low eddy diffusion coeffcients or low SO surface "sticking" probabilities. If this ratio is affected by volcanic activity, it could be temporally and/or spatially variable to the extent that the S/O ratio in the neutral clouds and plasma torus could be correlated with volcanic activity.

Moses *et al.* (2002b) concentrate on alkali and chlorine species, predicting that NaCl, Na, Cl, KCl, and K are the dominant alkali and chlorine species generated from Pele-type eruptions. Although they test the sensitivity of their results to different assumptions about the gas composition, these five species dominate for a wide range of conditions. Other sodium and chlorine molecules are minor constituents of the atmosphere because of their low volcanic source rates and efficient photochemical destruction. NaCl is not recycled efficiently, as its loss rate by photolysis greatly exceeds the volcanic production rate. Unless a surface sputtered source is important it will be rapidly depleted from the atmosphere, and therefore Moses *et al.* (2002b) conclude with confidence that it should be more readily apparent during periods of higher volcanic activity. The observed NaCl mixing ratio (Lellouch *et al.* 2003) in volcanic gases is somewhat lower than expected from these thermochemical models because of the large abundances assumed for Na and Cl, which were based on extrapolations of torus Cl ion abundances. Estimates of the escape flux based on the NaCl volcanic rates inferred by Lellouch *et al.* (2003) and the Moses *et al.* (2002b) prediction for the fate of the NaCl, suggest that most of it escapes in the form of atomic Na and Cl at a rate consistent with the supply rates to the torus, as inferred from neutral cloud and torus luminosities.

"Unified" Models

Although models have yet to capture the full complexity of Io's atmosphere, the first steps have now been taken to combine, to some degree, the vertical and horizontal calculations in a series of papers by Wong and co-workers (Wong and Johnson 1995, 1996a, Wong and Smyth 2000). In contrast to the previous vertically averaged or static columns, they used a fluid dynamics model to perform two-dimensional calculations assuming a sublimation-driven SO_2 atmosphere with axial symmetry about the subsolar point. The first paper focused primarily on illustrating the effect of plasma heating on the sublimation-driven flow, and estimating the exobase altitude and torus supply rate; plasma and solar UV heating were included, but Joule heating and chemistry were not. As in previous work (Lellouch *et al.* 1992, Strobel *et al.* 1994), Wong and Johnson (1995) found that plasma heating is most important near the exobase, and thus has important consequences for the overall dynamics of the atmosphere in the region which controls the loss of atoms and molecules. Wong and Johnson (1996a) extended the analysis using an improved fluid dynamics model that also included photochemistry and diffusion. This paper was concerned mainly with evaluating the suggestion that noncondensibles (O_2, and possibly SO) could accumulate and dominate the atmospheric dynamics, and the question of whether a nightside O_2 atmosphere could build up. O_2 is assumed to be noncondensible, while SO is in some cases assumed to be noncondensible and in others to be condensible. They find that the buildup of a nightside atmosphere of noncondensible photochemical products does not overwhelm the dayside atmospheric flow, but it does raise the overall atmospheric pressure and reduce the wind speed. Wong and Smyth (2000) considered high and low density SO_2 atmospheres at both both dawn and dusk elongation using an improved version of the multispecies hydrodynamic code. Assuming that O_2 and SO are both noncondensible, they find that gas-phase reactions among the noncondensibles can produce a substantial amount of SO_2 in the nightside atmosphere. They consider four cases (high and low density SO_2 atmospheres at both eastern and western elongation) and find for all cases considered that an exobase above the surface occurs globally (see Figure 19.8). The dayside SO/SO_2 mixing ratio is ~3–7 %, consistent with the SO measurements described above. The SO_2 subsolar column density in their models is always higher than the comparable hydrostatic sublimation atmosphere case, showing that the abundance of a sublimation atmosphere is dynamically controlled.

19.2.4 Synthesis

Our understanding of Io's atmosphere has improved radically in the nearly 30 years since its first detection. The current state of knowledge about it is summarized in Table 19.2. Since the detection of Na and the earliest models that assumed compositions of N_2, NH_3, CH_4, and Ne, nine species have now been directly detected (SO_2, S_2, SO, S, O, Na, K, NaCl, Cl) and via theoretical modeling others (especially O_2) are strongly suspected. From models of the SO_2 atmosphere that ranged over at least six orders of magnitude in surface pressure, the plethora of new observations obtained since 1990 reach a number of reassuringly consistent conclusions, the firmest being that Io's SO_2 atmosphere is tenuous but collisionally thick, and is temporally variable but permanently detectable on both its leading and trailing dayside hemispheres. This readily excludes the purely subsurface cold trap and purely sputtered models. Further, the spatially resolved spectra provide evidence for a decrease in gas pressure with increasing latitude, and at least modest (factor of 2–5) density enhancements over active plumes. This conclusion is supported by the structure seen in the Lyman-α images and the most recent UV spectroscopy, and is in fact not contradicted by any observation. The decrease in SO_2 abundance with latitude is consistent with Io's surface temperature being lower at the poles than at the terminators (as predicted by the most recent radiative equilibrium models) and/or with volcanoes preferentially located at low latitudes. As with SO_2 frost (Douté *et al.* 2001), SO_2 gas is ubiquitous on Io, except perhaps at the poles.

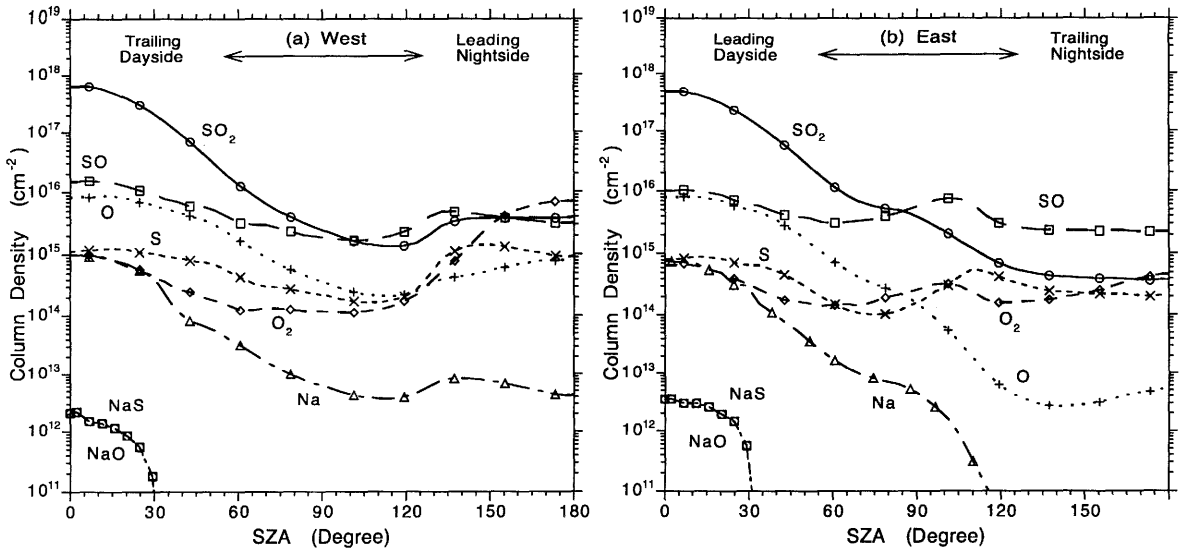

Figure 19.8. The variation of column density with solar zenith angle for various constituents of Io's atmosphere in the 2-D, axisymmetric models of Wong and Smyth (2000) assuming SO is noncondensible. Left-hand figure is for western elongation, right-hand figure is for eastern elongation. (From Wong and Smyth 2000, Figure 5).

Table 19.2. Summary of Io atmospheric species.

Species	Io Abundance*	Reference
SO_2	$\sim(1-10) \times 10^{16}$ in $\sim \pm(30-45)^\circ$ latitude band $\sim(2-10?) \times$ higher in active volcanoes	Synthesis of all observations; see Sections 19.2.2, 19.2.3, and 19.2.4; McGrath *et al.* 2000a; Spencer *et al.* 2000; Spencer *et al.* 2002; Jessup *et al.* 2004
S_2	1×10^{16}, Pele plume (t), $SO_2/S_2 \sim(3-12)$	Spencer *et al.* 2000
SO	$\sim(0.03-0.1) \times SO_2$	Lellouch 1996
NaCl	$(0.003-0.013) \times SO_2$, active volcanoes	Lellouch *et al.* 2003
O_2	Inferred (modeling)	Kumar (1982, 1985); Summers 1985; Summers and Strobel 1996; Wong and Johnson 1995, 1996; Wong and Smyth 2000; Moses *et al.* 2002a, 2002b
S	$3.6 \times 10^{12} < \mathcal{N}_S < 1.3 \times 10^{14}$ (t) $\sim 9 \times 10^{12}$ at $2\,R_{Io}$ (t) $= 0.1 \times$ O	Feaga *et al.* 2002 (upper limit revised up; see text) Wolven *et al.* 2001
O	$>(4-7) \times 10^{13}$, disk average $\sim 1 \times 10^{14}$ at $2\,R_{Io}$ (t) $= 11 \times$ S	Ballester 1989 Wolven *et al.* 2001
Na	4×10^{12}, disk average	Bouchez *et al.* 2000 [see also Burger *et al.* 2001, Retherford 2002]
K	$(1-10)\times 10^8$; Na/K $= 10 \pm 5$ at $(10-20)\,R_{Io}$	Brown 2001
Cl	$\sim 1 \times 10^{13}$, disk average	Feaga *et al.* (2004)
H	$\sim 2 \times 10^{12}$	Strobel and Wolven 2001
CS_2	$<2 \times 10^{14}$	McGrath *et al.* 2000a; Spencer *et al.* 2000; Spencer *et al.* 2002
CO	$<(3.6-6) \times 10^{17}$	Lellouch *et al.* 1992
H_2S	$<(0.7-1.2) \times 10^{16}$	Lellouch *et al.* 1992
OCS, S_2O, ClO, CS, NaOH	Not detected (mm)	Lellouch *et al.* 1992
KCl	$<1 \times$ NaCl	Lellouch *et al.* 2003

* Numbers in vertical column density, cm^{-2}, unless otherwise noted; (t) = tangential.

Most current evidence favors the [larger fractional coverage, smaller column abundance] regime as opposed to the [smaller fractional coverage, higher column abundance] regime. There is little compelling evidence for very large, localized enhancements except for the *Voyager* IRIS observation of Loki, and even that can be explained with a significantly lower column abundance than initially estimated (Lellouch *et al.* 1992). SO_2 column densities inferred in the Pele plume from spatially resolved spectroscopy and imaging are in remarkable agreement at a value of $\sim 3 \times 10^{16}\,\mathrm{cm}^{-2}$. Thus, the emerging view is that of an SO_2 atmosphere with a mean $\sim(1-10) \times 10^{16}\,\mathrm{cm}^{-2}$ column, covering typically 50–70% of Io's dayside surface, mostly but not exclusively at low latitudes, with lateral variations encompassing a total factor of $\sim 10-100$.

However, as has been the case with Io's atmosphere from the very beginning, it is currently not possible to reconcile all the observations. The "hydrostatic" interpretation of the millimeter observations of an atmosphere distributed in much denser and more localized centers, especially on the trailing side ($f_h = 2.5$–$8\,\%$), is not consistent with the above picture. The extreme patchiness is relaxed in the "volcanic plume" interpretation, and larger surface coverages ($f_h > 30\%$) are obtained when low gas temperatures (<200 K) are assumed. This requires the atmosphere to be dominated by direct output from ten to perhaps 200 volcanic centers. While it is difficult to assess the plausibility of such large numbers, it is worth emphasizing that we now have several direct indications that Io's atmosphere is at least partly volcanic, including (i) the detection of SO_2 in Pele's plume at the limb (i.e., near the terminator, where the surface temperature is probably too low for a sublimation component); (ii) the detections of S_2 and NaCl, both of which have short lifetimes in a hydrostatic atmosphere; (iii) the detection of the forbidden infrared SO band; and (iv) the temporal variability seen in the millimeter and Lyman-α data and inferred from several other observations.

With typical sublimation rates of $1\,\mathrm{mm\,yr}^{-1}$ and an SO_2 ice layer at least several centimeters thick (Schmitt *et al.* 1994), a sublimation atmosphere is expected to be relatively stable, whereas an atmosphere supplied by a large number of simultaneous volcanic plumes implies temporal variability. Volcanoes not only produce local atmospheres within the plumes, they also serve to maintain the frosts. All this suggests that the volcanic interpretation of the millimeter data should be preferred. *A contrario*, the widespread atmosphere seen in the HST spectra and Lyman-α images may imply a sublimation component, although these data are inconsistent with an atmosphere that is azimuthally symmetric about the subsolar point. While plume-like models have not been used in fitting the UV data, it can be anticipated that they would lead to slightly higher SO_2 columns, since these models include large column density variations on unresolved (<100 km) scales. Preliminary assessment of the effect on the analysis of the Lyman-α data suggests an $\sim$50% increase in the SO_2 column, allowing further reconciliation with the millimeter data.

A discrepancy remains with the *Galileo*/UVS data, which depict Io's atmosphere as consisting of two components, each of which is much denser than in the HST picture. If the spectral structure seen at 2200–2800 Å is due to SO_2 gas, it is inevitable to find very high SO_2 columns as the SO_2 cross section in this range is less than $\sim 1 \times 10^{-18}$ cm^2. It is also possible that the broadband structure is due to the surface reflectance of materials other than SO_2 frost, which is the only surface component used in the models. SO_2 patches with columns of 1×10^{19} and even $4 \times 10^{17}\,\mathrm{cm}^{-2}$ would be invisible (saturated out) at 2000–2200 Å and appear as black areas at Lyman-α. This may not be inconsistent if these dense patches are smaller than the $\sim$200 km resolution limit of the Lyman-α images. Conversely, the $\lesssim 10^{17}\,\mathrm{cm}^{-2}$ columns inferred from HST are undetectable in the UVS range.

The least well constrained parameter is the characteristic gas temperature. The Keck II observation of SO indicates that at least a fraction of the volcanic gas is hot (1000 K) – implying that the thermodynamics of eruptive plumes are more complex than a mere adiabatic expansion. In the millimeter, the hydrostatic interpretation of the best data gives $T_{\mathrm{atm}} = 200\,\mathrm{K}$ on the leading side and $T_{\mathrm{atm}} = 400\,\mathrm{K}$ on the trailing, but the preferred volcanic interpretation does not constrain the gas temperature. In the interpretation of the UV data, while many authors have simply assumed values for T_{atm}, the temperatures inferred by Ballester *et al.* (1994), McGrath *et al.* (2000a), and Spencer *et al.* (2000) range from 110 to 500 K, with a general preference for 200–300 K. This problem is formidably difficult, especially for a volcanic atmosphere which is expected to exhibit huge lateral temperature variations.

Despite considerable progress in the past 13 years, many questions remain, including a quantitative understanding of how variable the atmosphere is, whether such variability can be related to changes in the Io plasma torus, what the nightside atmosphere is like, and what happens to the atmosphere in eclipse. Further progress would be facilitated by new measurements of the SO_2 frost reflectivity at 1200–3000 Å and reflectivities of other surface components are needed so that uncertainties in the interpretation of the UV data can be addressed. Although it is again formidable, true 3-D calculations, in which the assumption of axial symmetry about the subsolar point is relaxed, are now warranted by the observations. Electron excitation cross sections and rate coefficients are desperately needed to improve estimates of the atomic sulfur and chlorine densities in Io's atmosphere.

19.3 EUROPA, GANYMEDE, AND CALLISTO

19.3.1 Early Work

Early work strongly suggested that the surfaces of Europa, Ganymede and Callisto are covered mainly with H_2O frost (Kuiper 1957, Moroz 1961, Lewis 1971), which was first confirmed by the positive identification of H_2O features by Pilcher *et al.* (1972). The subsequent report of an approximately 1 μbar atmosphere on Ganymede from a stellar occultation measurement (Carlson *et al.* 1973) motivated Yung and McElroy (1977) to develop a photochemical model of a sublimation-driven water ice atmosphere, which evolves into a stable molecular oxygen atmosphere by photolysis of H_2O because the hydrogen preferentially escapes. In their model, nonthermal escape of O atoms balances the production of O_2 to yield a surface pressure of $\sim$1 μbar consistent with the Carlson *et al.* (1973) measurement. They reached several

conclusions: Ganymede should have an appreciable oxygen atmosphere as long as the partial pressure of atmospheric H_2O exceeds about 2×10^{-9} mbar, which occurs for surface temperatures $\gtrsim$134 K; it should have a Lyman-α halo produced by resonance scattering of sunlight by the escaping hydrogen; and an O_2 atmosphere should have a significant ionosphere produced by photoionization of O and O_2 with a peak electron density of 2×10^4 cm^{-3}. Yung and McElroy also concluded that the higher albedo of Europa would inhibit sublimation, suppressing the formation of O_2; Callisto they deemed more promising because its surface temperature is higher. Kumar and Hunten (1982) pointed out that this model possessed an additional stable solution with a much lower surface pressure of $\sim 10^{-6}$ μbar. *Voyager 1* Ultraviolet Spectrometer stellar occultation measurements of Ganymede yielded an upper limit on the surface pressure of 10^{-5} μbar (Broadfoot *et al.* 1979), compatible only with the low pressure solution.

Prior to the *Voyager 1* encounter with Jupiter, there was little appreciation of the importance of sputter generated atmospheres/exospheres. Significant advances were made in understanding sputtering processes by innovative laboratory studies (Lanzerotti *et al.* 1978, Brown *et al.* 1980, Johnson *et al.* 1983) and in application of these results to planetary systems (Johnson *et al.* 1982, Wolff and Mendis 1983). Based on laboratory data, Lanzerotti *et al.* (1978) suggested that bombardment of the satellite surfaces by the jovian plasma leads to an erosion rate on Ganymede that could support the H_2O partial pressure used by Yung and McElroy (1977). The rates would be much larger at Europa, but much smaller at Callisto. Subsequent laboratory data showed that O_2 is directly produced in and ejected from ice (Brown *et al.* 1980), a process referred to as radiolysis (see Chapter 20). Using these data, Johnson *et al.* (1982) estimated that O_2 sputtered from water ice on Europa could yield a bound atmosphere with a column density $\mathcal{N}_{O_2} \sim$ 2–3 $\times 10^{15}$ cm^{-2}. Since O_2, does not stick efficiently at these temperatures and does not escape efficiently, the atmosphere is dominated by O_2, even though the sputtered flux of H_2O molecules is larger than that of O_2.

Wolff and Mendis (1983) assumed the basic validity of the Yung and McElroy (1977) model with water ice sublimation as the source of icy Galilean satellite atmospheres and estimated O_2 atmospheres with surface densities in the range of 10^{10}–10^{14} cm^{-3}, even though the *Voyager* UVS observations excluded such high densities on Ganymede and Callisto (Broadfoot *et al.* 1979, 1981) as pointed out by Eviatar *et al.* (1985). For Europa, assuming a sticking coefficient of 1.5×10^{-3} for O_2, Eviatar *et al.* (1985) calculated that the exobase is on Europa's surface, and they estimated that the "atmosphere" is a sputtered O_2 exosphere with column density $\sim 1 \times 10^{14}$ cm^{-2}.

19.3.2 Europa

Oxygen Atmosphere and Ionosphere

The first detection of Europa's atmosphere was accomplished using HST/GHRS by Hall *et al.* (1995), who discovered the semi-forbidden OI (^{5}S°–^{3}P)1356 Å and optically allowed OI (^{3}S°–^{3}P)1304 Å multiplets in emission (Figure 19.9). The observed intensity ratio, I(1356)/I(1304), was

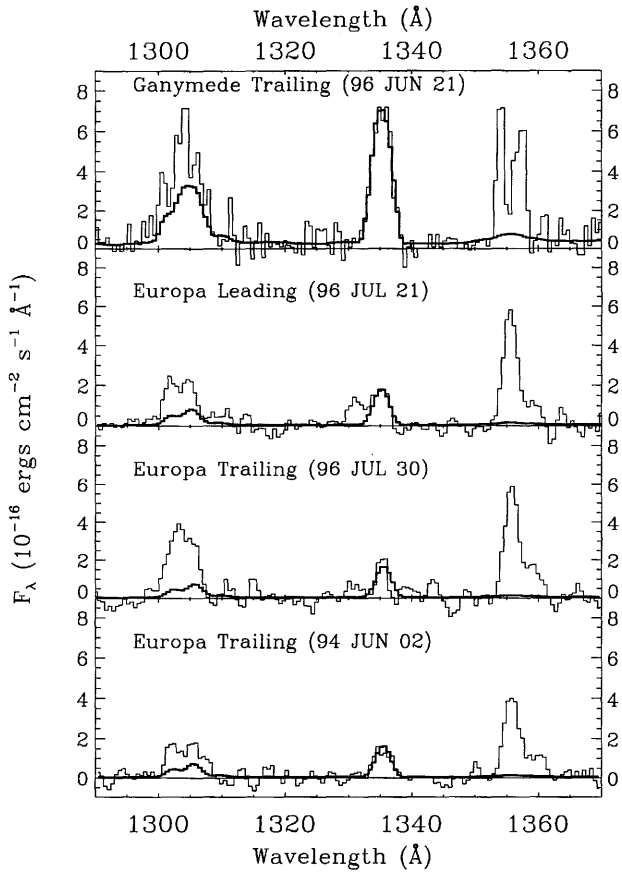

Figure 19.9. The Hall *et al.* (1998) detections of electron excited oxygen emission at 1304 and 1356 Å from Europa and Ganymede, indicating O_2 atmospheres on these satellites. The features at 1335 Å are due to solar C^+ emission reflected from the surfaces.

$\sim$1.9:1. They interpreted this as evidence for electron impact dissociative excitation of O_2 as the dominant excitation mechanism. The other plausible sources of the observed OI multiplets, solar resonance fluorescence scattering by O atoms and reflection of solar UV light from the surface, produce negligibly small intensities. The inference that Europa's atmosphere is O_2 and not O is based on the I(1356)/I(1304) ratio. Noren *et al.* (2001) have provided accurate electron impact cross sections for these dissociative excitations. For a Maxwellian distribution of electrons over a broad energy range this intensity ratio is 2. By contrast, incorporating the OI 1304 Å cross section of Doering and Yang (2001), the I(1356)/I(1304) ratio for O atoms has a broad maximum of 0.35 at 4 eV.

The absolute intensities imply a molecular oxygen atmosphere with column density $1.5 \pm 0.5 \times 10^{15}$ cm^{-2} ($P_0 = 2.2 \pm 0.7 \times 10^{-6}$ μbar) on the trailing hemisphere of Europa, which is consistent with the early estimate of a bound atmosphere by Johnson *et al.* (1982) and the low pressure solution discussed by Kumar and Hunten (1982). In deriving the O_2 column density, Hall *et al.* (1995) assumed: the spatial distribution of Europa's atmosphere is confined to the geometric cross section of the observed hemisphere (i.e., the scale height of the atmosphere is significantly smaller than the radius of Europa); a negligible contribution to the observed flux is emitted from above the tangential limb along

the terminator; the Io plasma torus electrons responsible for exciting the observed emissions interact with the atmosphere without energy degradation; and no electrodynamic, sub-Alfvénic interactions such as observed by *Voyager* at Io (e.g., Ness *et al.* 1979, Neubauer 1980) were considered. The oxygen atmosphere has been confirmed with additional HST/GHRS observations of both the trailing and leading hemispheres by Hall *et al.* (1998) (Figure 19.9). With a finite scale height and emission above the limb included, the inferred molecular oxygen column densities are in the range $\sim(2.4\text{–}14) \times 10^{14}\,\mathrm{cm}^{-2}$.

Ip (1996) published an exospheric model for the O_2 atmosphere on Europa that included deflection of the incident plasma. He assumed that the atmosphere is created predominantly by magnetospheric thermal ion sputtering of O_2 from water ice. However, his calculated exospheric column density failed by more than a factor of 1000 to account for the inferred O_2 column density. He therefore invoked additional surface sputtering by newly ionized O_2 molecules accelerated by the corotational electric field and convected back into Europa's surface from which they had only recently been sputtered. According to Ip this "resputtering" mechanism is sufficient to raise the density of the gravitationally bound O_2 molecules past the threshold value that defines the transition from an exosphere to an atmosphere.

Based on the HST observations and the previous modeling attempts, Saur *et al.* (1998) developed a plasma interaction model to account for the sources and sinks of the neutral atmosphere, and to describe the interaction of the jovian magnetosphere with the atmosphere and the formation of an ionosphere. They found that suprathermal torus ions plus a contribution from thermal ions could sputter O_2 from the water ice surface to create an atmosphere that is in mass balance with thermal ion stripping of the O_2 atmosphere by charge exchange and atmospheric sputtering. Using the sputtering rates of Shi *et al.* (1995), which are based on *Voyager* plasma measurements, an average O_2 column density of $\sim(3\text{–}7) \times 10^{14}\,\mathrm{cm}^{-2}$ can be maintained. With this O_2 column density, they calculated intensities of the OI 1356 and 1304 multiplets in agreement with those observed by Hall *et al.* (1995). Europa's "equilibrium" atmosphere is strongly influenced by the electrodynamic interaction. The magnetospheric ions that create the atmosphere experience a reduced effective geometric area for Europa as the plasma flow is shielded (Goertz 1980). As the atmospheric density increases, the ionospheric densities and conductivities are enhanced, leading to larger electric currents and reduced ionospheric electric fields. The resulting enhanced shielding reduces the sputtering rate. Stripping of the O_2 atmosphere by charge exchange and atmospheric sputtering increases initially at low atmospheric density and asymptotically approaches a constant rate consistent with a finite plasma power reservoir. Mass balance is achieved at the above column density range with atmospheric creation and removal rates of $\sim 10^{27}\,\mathrm{s}^{-1}$ (see their Figure 2). Ionization of O_2 molecules followed by pickup and convection out of the atmosphere accounts for only 15 % of the atmospheric loss rate. Saur *et al.* (1998) showed that the Ip (1996) "resputtering" mechanism could contribute only $\sim$0.005 of the total sputtering rate on Europa because ionospheric ions have low energy and sputtering yields.

Shematovich and Johnson (2001) have carried out a 1-D Monte Carlo simulation of Europa's oxygen atmosphere. Representative molecules were ejected from the surface and followed between collisions, accounting for surface accomodation, dissociation and ionization by solar UV and magnetospheric electrons, and collisonal ejection by the incident plasma. The non-thermal as well as thermalized O_2 were tracked, as were the energetic O atoms produced by dissociation. They used a recent set of cross sections for collisional dissociation and ejection of O_2 (Johnson *et al.* 2001). The atmospheric density, temperature and escape flux were calculated as a function of the surface source rate. They found that the atmosphere was not well approximated by the simple model in Saur *et al.* (1998), but they obtained a source rate required to match the oxygen observations that was comparable (Shematovich *et al.* 2004).

Using the *Galileo* plasma measurements, Cooper *et al.* (2001) carried out a comprehensive study of the effects of energetic ion and electron irradiation of the icy surfaces of the Galilean satellites. In their Table II they give an ion sputtering timescale for Europa of $6.1 \times 10^4\,\mathrm{yr\ mm}^{-1}$, which is dominated by energetic oxygen and sulfur ions. When converted to a sputtered flux of $1.8 \times 10^9\,\mathrm{cm}^{-2}\,\mathrm{s}^{-1}$ and multiplied by the surface area of Europa, one gets $5.6 \times 10^{26}\,\mathrm{s}^{-1}$ for the direct H_2O sputtering rate. Like the results in Shi *et al.* (1995) this is a lower bound to the sputtering rate which depends on temperature above 100 K. This result is much smaller than the Shi *et al.* (1995) H_2O sputtering rate of $\sim 3 \times 10^{28}\,\mathrm{s}^{-1}$. The latter was based on *Voyager* measurements for which the suprathermal plasma was presumed to be predominatly heavy ions. However, the *Galileo* measurements clearly show that the ion energy flux to the surface is predominantly carried by the energetic protons and electrons (Cooper *et al.* 2001, Paranicas *et al.* 2001, 2002) which do not sputter as efficiently. The reduction of the H_2O yields due to surface porosity (Johnson 1989) is roughly accounted for in these estimates. Because the sputter-produced O_2 does not stick to neighboring grains there is no reduction for porosity, enhancing its relative source strength (see Chapter 20).

An ionosphere has also been detected on Europa. Kliore *et al.* (1997, 2001a) characterize results from the eight *Galileo* radio occultation measurements at Europa as five strong detections, two weak detections, and one non-detection of an ionosphere. They conclude on the basis of the various geometries for the angle, Ψ, between the center of the trailing hemisphere (the sub-ram point) and the subsolar point that a necessary condition for detection of an ionosphere is that the trailing hemisphere must be partially solar illuminated, i.e., $\Psi < 90°$. The non-detection of an ionosphere in the E26 flyby entry occultation was at high latitude and in the wake region, where according to the plasma model of Saur *et al.* (1998) the ionosphere of Europa becomes detached from the satellite as it convects downstream (cf. their Fig. 7). Spherical symmetry, which is assumed in all analyses of ionospheric occultations, is then no longer applicable and the occultation geometry does not yield a Chapman factor column density enhancement of $(2\pi R/H_\mathrm{p})^{0.5} \sim 10$, where R is the satellite radius and H_p is the plasma scale height.

Saur *et al.* (1998) found that electron impact ionization can generate Europa's ionosphere at the electron densities measured by Kliore *et al.* (1997, 2001a). The total ionization

rate ($\sim 10^{26}\,\mathrm{cm^{-2}\,s^{-1}}$) is limited by the finite power supplied to the ionosphere by electron heat conduction along magnetospheric flux tubes that interact with Europa's atmosphere. In their calculation they adopted typical *Voyager* magnetospheric plasma conditions at Europa: $n_e = 38\,\mathrm{cm^{-3}}$ and $2\,\mathrm{cm^{-3}}$ at $T_e = 20\,\mathrm{eV}$ and 250 eV, respectively. The electron impact ionization rate is $1.9 \times 10^{-6}\,\mathrm{s^{-1}}$, which may be compared to a solar maximum photoionization rate of $6 \times 10^{-8}\,\mathrm{s^{-1}}$. It should be noted that the intrinsic time constants associated with these processes are 6 and 190 days, respectively, which should be compared with Europa's 3.6-day orbital period. Thus the solar photoionization rate should be diurnally averaged (a factor of 0.5 for Europa's optically thin atmosphere), whereas electron impact ionization depends mostly on ambient magnetospheric plasma densities. In order for photoionization to be competitive with electron impact ionization, the magnetospheric electron density would have to be $\lesssim 1\,\mathrm{cm^{-3}}$. Thus in the case of Europa, it is difficult to understand why the existence of an ionosphere depends on solar illumination. For the Europa radio occultations observed in *Galileo* orbits E4 and E6, the ambient magnetospheric ion densities were $\sim$25 and $15\,\mathrm{cm^{-3}}$, respectively (Paterson *et al.* 1999), and the corresponding electron densities would be about 50% larger. Kurth *et al.* (2001) suggest that a typical torus electron density is $80\,\mathrm{cm^{-3}}$ at the orbit of Europa.

Even more problematic is the lack of an ionospheric signature in the Paterson *et al.* (1999) and Gurnett *et al.* (1998) data for Europa's wake region during the E4 flyby. Because ionospheric plasma should presumably be $\mathbf{E} \times \mathbf{B}$ convected downstream, Paterson *et al.* (1999) and Gurnett *et al.* (1998) should have detected plasma densities commensurate with the magnitude of the electron densities inferred by Kliore *et al.* (1997, 2001a). The plasma model of Saur *et al.* (1998) yielded reduced plasma velocities of $\sim 20\,\mathrm{km\,s^{-1}}$ in the vicinity of Europa. If the peak density in the E4 wake data of Paterson *et al.* (1999) were interpreted as O_2^+, then the ion (and electron) density is at most $\sim 110\,\mathrm{cm^{-3}}$ with speed $\sim$50 km/s. Similarly, Gurnett *et al.* (1998) found electron density enhancements of 50–100 electrons $\mathrm{cm^{-3}}$ above the approximately 80 torus electrons $\mathrm{cm^{-3}}$ at Europa's orbit during the E4 flyby. Kurth *et al.* (2001) report plasma wave observations for the nine *Galileo* spacecraft close flybys of Europa. The maximum density enhancement observed on any flyby was on the E15 flyby when the electron density jumped from 200 to $400\,\mathrm{cm^{-3}}$ as the spacecraft entered the wake. Because the E4 flyby was the closest to Europa in the wake, our analysis focuses on this flyby. The downstream distance from Europa is $\sim$2000 km and the transit time is at most 100 s. An initial ionospheric parcel with $n_e = 10^4\,\mathrm{cm^{-3}}$ will require $\sim 10^4$ s to recombine dissociatively to a density of $1000\,\mathrm{cm^{-3}}$, but almost an additional 10^5 s to decrease from 1000 to $100\,\mathrm{cm^{-3}}$, as the recombination rate is proportional to n_e^2. To convect a distance of 2000 km in 10^4 and 10^5 s demands plasma speeds of 0.2 and 0.02 $\mathrm{km\,s^{-1}}$, respectively, completely out of the observational and modeling range of 20–100 $\mathrm{km\,s^{-1}}$.

Recent HST/STIS images in the OI multiplets (Figure 19.10) indicate a more complex pattern of emission than would be expected from plasma interaction with an optically thin atmosphere. The McGrath *et al.* (2000b) OI 1356 image displays the expected limb glow around the disk plus a much

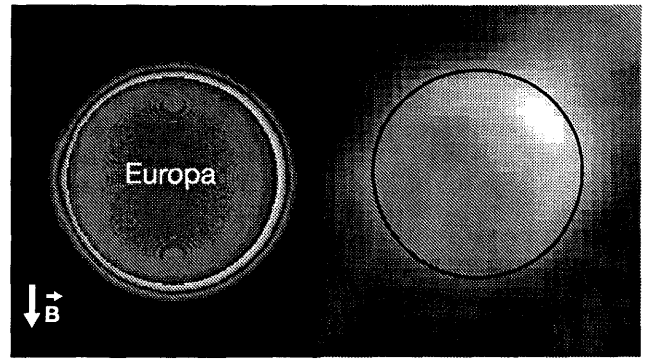

Figure 19.10. Brightness from Saur *et al.* (1998) model (left) compared with recent HST/STIS OI 1356 Å image of Europa.

brighter region on the anti-jovian hemisphere. Shown for comparison is the calculated intensity pattern from the Saur *et al.* (1998) model which emphasizes the bright limb glow due to the long tangential path length above the limb. The STIS point spread function will degrade the sharpness of predicted limb glow to the more diffuse glow seen in the STIS image. It is difficult to understand why the brightest region is on the disk due to its reduced path length. Since Europa has a weak induced magnetic field (Kivelson *et al.* 1997), it is not capable of focusing jovian electrons or energetic ions with finite gyroradii which sputter molecules into localized regions. It would be much easier to understand the bright region if it were on the limb in an asymmetric atmosphere with larger abundance on the anti-jovian side and the same physics that produces Io's equatorial bright spots, where the brighter one is on the anti-jovian side. The observation of localized O emission may suggest that the surface is not icy everywhere, as assumed in the models described above, but rather that the composition varies considerably with longitude.

In summary, the HST observations of Hall *et al.* (1995, 1998) and the ionospheric radio occultations of Kliore *et al.* (1997, 2001a) lead to a consistent description of Europa's atmosphere with the interpretive aid of a model that includes plasma deflection like that of Saur *et al.* (1998). It should be emphasized that the ratio of the ion drag force due to plasma flow through Europa's atmosphere to the gravity force $\langle \sigma \times v_i \rangle\, n_i\, v_i / g$ is large ($\sim$4), for 10^4 electron $\mathrm{cm^{-3}}$ and $v_i \sim 50\,\mathrm{km\,s^{-1}}$, where a typical collision rate for O_2^+ with O_2 of $\langle \sigma \times v_i \rangle$ is $\sim 10^{-8}\,\mathrm{cm^3\,s^{-1}}$. Consequently, ionospheric plasma should be convected downstream, yet plasma observations by Paterson *et al.* (1999) and Gurnett *et al.* (2001) have not detected an Io-like ionospheric wake.

Alkalis at Europa

Both Na and K have been observed at Europa (Brown and Hill 1996, Brown 2001) and they occur in a ratio both very different from that at Io, and from the meteoritic or solar abundance ratios (Brown 2001, Johnson *et al.* 2002). The description of the sodium cloud at Europa is simpler than it is at Io because Europa has a much thinner atmosphere, where collisions are few and atoms ejected from the surface can directly escape. The morphology of the observed sodium cloud can therefore be used to constrain the ejecta velocity distributions and to directly estimate the surface source rate

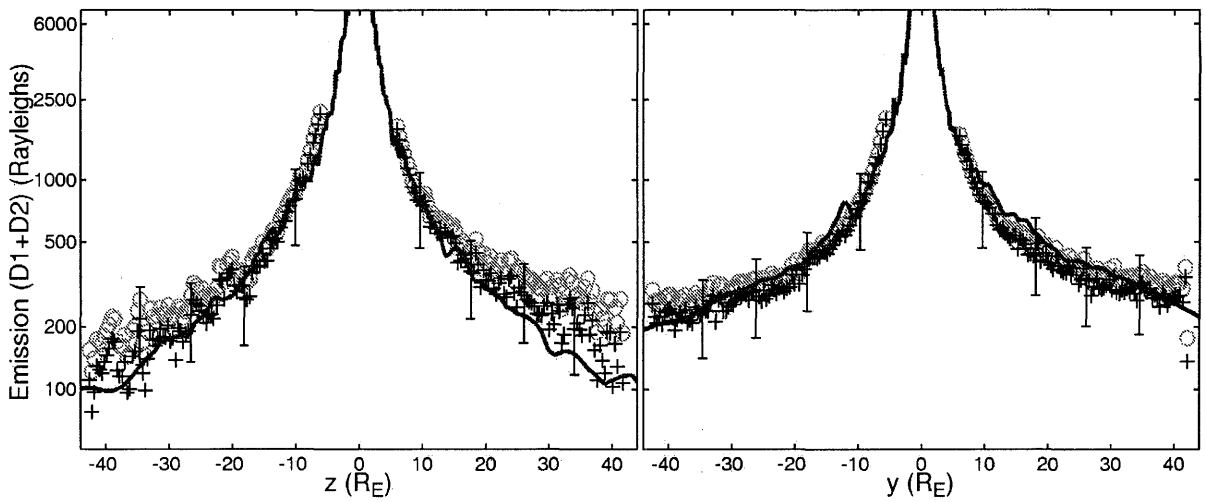

Figure 19.11. The Na intensity observed in N–S (left) and E–W scans of Europa compared with the model (solid line) of Leblanc *et al.* (2002) described in the text. Crosses include a background subtraction, open circles do not. From Figure 8 of Leblanc *et al.* (2002).

and the alkali concentration in the surface (Johnson 2000). Leblanc *et al.* (2002) have produced a model of the sodium cloud at Europa (Figure 19.11) which is consistent with the observations. The model used to create Figure 19.11 includes the gravity of Jupiter, giving a banana-shaped cloud like that at Io (Smyth and Combi 1997), and solar radiation pressure, which stretches the cloud in the direction away from the Sun. Since most of the ejected Na and K atoms return to the surface, the alkalis are efficiently redistributed across Europa's surface from their initial source region. By fitting to Brown's observations, a source rate is obtained, as well as the velocity distribution for sodium ejected from the surface. Quite remarkably, the velocity distribution obtained is very similar to that recently measured by Yakshinskiy and Madey (1999, 2001) for alkalis ejected from ice by electronic sputtering. Using this model the Na/K ratio close to Europa has been estimated (Johnson *et al.* 2002). The average surface concentration of Na is ~0.5% and the required source of sodium is larger than that supplied by micrometeorites or by plasma ion implantation from Io. Since the Na/K ratio also differs from that at Io (Brown 2001), a subsurface source of alkalis is suggested. The Na/K ratio at Europa, though somewhat higher than predicted by models of a subsurface ocean, is not inconsistent with fractionation during transport to the surface (Zolotov and Shock 2001). The observed alkalis may therefore be the first direct detection of material from Europa's subsurface ocean.

19.3.3 Ganymede

Hall *et al.* (1998) also discovered an atmosphere on Ganymede via HST/GHRS observations of the same oxygen multiplets observed on Europa (Figure 19.9). As for Europa, the intensity ratio OI 1356/OI 1304 of ~1.3 implies a predominantly O_2 atmosphere. They estimated molecular oxygen column densities in the range of $\sim(1\text{–}10)\times10^{14}\,\mathrm{cm}^{-2}$. The OI 1356 multiplet structure exhibited a doubly-peaked profile that implied non-uniform spatial emission consistent with two distinct polar cap regions. These regions were thought to correspond to the loci of open field lines of Ganymede's intrinsic magnetic field (Kivelson *et al.* 1996). The spatial distribution of the oxygen emission was clarified by the HST/STIS observations of Feldman *et al.* (2000a) (Figure 19.12), which indicate that the brightest Ganymede OI emissions are auroral in a manner analogous to the Earth's highly variable auroral oval regions. They correspond to regions where electrons trapped inside Ganymede's magnetosphere can be accelerated down field lines into the atmosphere to generate high conductivity and luminosity.

Based on excitation rates for Maxwellian electrons in the range T_e = 10–20 eV, we estimate the OI red line at 6300 Å should be about 10 times as bright as OI 1356 Å. Brown and Bouchez (1999) used the Keck telescope to detect the OI red lines (6300 Å, 6364 Å) when Ganymede was in eclipse. The estimated red line intensity of 1–2 kR is consistent with STIS inferred intensities for OI 1356 Å. They observed two "spots" near opposite limbs at low latitudes, however, the spatial resolution is only ~1 Ganymede radius, making it difficult to directly compare the morphology with the STIS observations. Although polar spots can be ruled out, the observed spots could be equatorial atmospheric limb emission confined to regions with closed magnetic field lines or alternatively, the mid-latitude "auroral oval" emission patterns such as those seen in the HST/STIS observations.

Barth *et al.* (1997) measured HI Lyman-α emission from Ganymede's atmosphere of 0.56 kR with the *Galileo* Ultraviolet Spectrometer. From the radial intensity profile, they deduced an H atom density of $1.5\times10^4\,\mathrm{cm}^{-3}$ at the surface with exospheric scale height equal to 1 Ganymede radius (= 2634 km) and temperature of 450 K. Feldman *et al.* (2000a) also detected Lyman-α emission in their HST/STIS observations. Their radial intensity profile, and hence density profile, was in excellent agreement with the Barth *et al.* (1997) data.

Unlike Europa, Na has not been detected at Ganymede. Long-slit high resolution spectra obtained by Brown (1997) provide only an upper limit of 10^8 atoms/cm^2 between 7800 and 15 600 km from the satellite surface, which is 13 times smaller than the Na density at the same distance from the surface of Europa. This is roughly consistent with the lower sputtering rates (e.g., Cooper *et al.* 2001) and higher es-

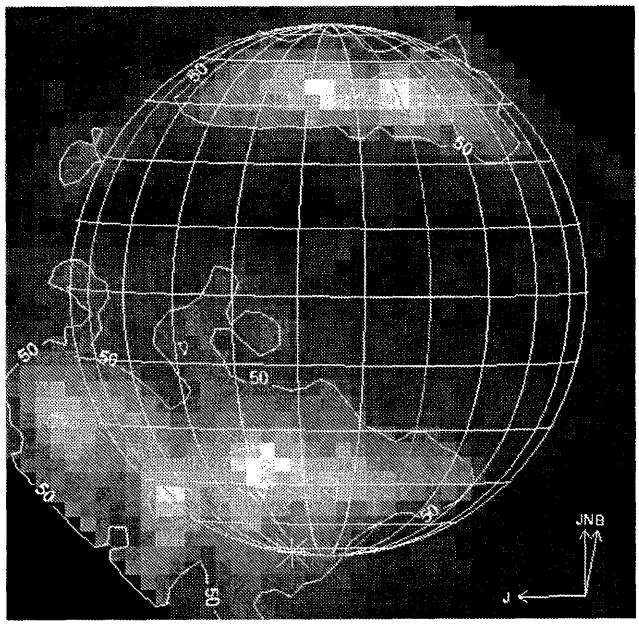

Figure 19.12. Ganymede auroral emission from oxygen (OI 1356 Å) observed with HST. Contours illustrate the observed brightness in Rayleighs.

cape energies for Ganymede, but also likely means that the concentration of Na on the surface is much smaller on Ganymede than on Europa.

In sharp contrast to Europa, Kliore *et al.* (2001b) reported only one strong detection, two weak detections, and 5 non-detections of an ionosphere via *Galileo* radio occultation measurements. Most of these occultation observations occurred at low latitudes where Ganymede's magnetic field dominates and the field lines are closed. Two occultations occurred at latitudes of 47–49° in the vicinity of the separatrix region, but with an angle $\Psi \sim 148°$. The strong detection and one of the weak detections occurred at a latitude of 20° and $\Psi = 48°$, but no ionosphere was detected at latitude −7° and $\Psi = 68°$. The other weak detection occurred at latitude −25° and $\Psi = 94°$ for the entry occultation, but not for the exit occultation. Thus the requirement of $\Psi < 90°$ (which corresponds to partial solar illumination) applies to the strong detection but is marginally violated by the weak detection for $\Psi = 94°$.

Ganymede, with its intrinsic magnetic field, presents a bigger challenge to constraining or inferring the O_2 column abundance. A distinct polar limb glow would provide the best inference of O_2 column densities. Because the intensity ratio of the OI multiplets is consistent with electron impact on O_2, the inferred O_2 abundance depends on the electron density and energy distribution function. The broad polar caps on Ganymede (latitude >45°) are open to jovian plasma. The plasma densities and distribution functions have been measured by both *Voyager* and *Galileo* plasma instruments (Scudder *et al.* 1981, Paterson *et al.* 1999). *Voyager* measurements in the plasma sheet found enhanced densities ($\sim$5–20 cm^{-3}) with $T_e \sim 20$ eV, and a suprathermal tail at 2 keV and 0.1 times the core density (Scudder *et al.* 1981). This enhanced electron population could support OI 1356 Å limb glow of 10–40 R in an atmosphere constrained by an upper limit deduced from a *Voyager* UV stellar occultation (Broadfoot *et al.* 1981). However, the STIS observations display polar limb glow in the range 50–100 R, suggesting that more than plasma sheet electrons are involved in the excitation process.

The latter point is more evident when an explanation is sought for the hot spots of intense auroral emission seen in the HST/STIS observations (see Figure 19.12 and Figure 3 of Feldman *et al.* 2000a). Eviatar *et al.* (2001) addressed this question by asking how many electrons at what temperature are needed to generate one of the observed 300 R bright spots. They found a threshold electron number density of 310 cm^{-3} at $T_e \sim 100$–200 eV, more than an order of magnitude larger than the densities and temperatures measured in the plasma sheet. The hot spots could be produced by higher density, lower temperature electrons (e.g., $n_e = 2500$ cm^{-3} and $T_e = 8$ eV). All of these values pertain to an atmosphere ($\mathcal{N}_{O_2} = 2.5 \times 10^{14}$ cm^{-2}) that satisfies the *Voyager* UV stellar occultation upper limit. Eviatar *et al.* argued that in the absence of any measured electron population to produce the auroral hot spots, local acceleration of plasma is required. They identified stochastic acceleration by electrostatic waves and/or magnetic field-aligned electric fields with associated Birkeland currents as possible mechanisms. The hot spots are then regions of high electron density ($\sim 10^5$ cm^{-3}), high conductance ($\lesssim 100$ mho), and high "auroral electrojet" currents, all features of the Earth's auroral oval. The regions of high electron density would not be detectable by radio occultation measurements because of their limited spatial dimensions. One other potential solution to understanding the high HST intensities is to argue that the *Voyager* UV stellar occultation measurements are not applicable to the *Galileo*/HST epoch and atmospheric column densities are perhaps an order of magnitude larger, $\sim 3 \times 10^{15}$ cm^{-2}, which is the column density that stops 20 eV electrons.

In summary, our limited information prevents a definitive inference of the average O_2 column density on Ganymede. It is improbable that it is less than 10^{14} cm^{-2} to account for the HST intensities and debatable that it exceeds 3×10^{15} cm^{-2} in the polar cap regions.

19.3.4 Callisto

Much less is known about the atmosphere of the most distant Galilean satellite, Callisto. However, several recent results bear on this question. The first is the report by Carlson (1999) of a *Galileo* NIMS observation of limb emission from the 4.26 μm ν_3 fundamental stretching band of CO_2 up to an altitude of 100 km above the surface of Callisto (Figure 19.13). The geometry of the observation was such that it mapped a region tangential to the limb very near the equator and near noon, in the wake region of the plasma flow relative to Callisto. The observed emission was attributed to resonance fluorescence of sunlight by atmospheric CO_2. Modeling the data assuming an isothermal atmosphere, the best fit was obtained for a temperature of 150 K (close to the measured noon surface temperature of Hanel *et al.* 1979, Spencer 1987) and surface pressure of 7.5 pbar. The scale height of the assumed exponential atmosphere is 23 km, and the surface number density is $\sim 4 \times 10^8$ cm^{-3}, implying a vertical CO_2 column abundance of $\sim 8 \times 10^{14}$ cm^{-2} with estimated errors of about ±60%. This is comparable to the

Table 19.3. Summary of Europa, Ganymede, and callisto atmospheric species.

Species	Europa*	Ref.	Ganymede	Ref.	Callisto	Ref.
O_2	$(2.4–14) \times 10^{14}$	1	$(1–10) \times 10^{14}$	1	3×10^{16}	6
	$(3–7) \times 10^{14}$	2			(inferred, ionosphere)	
CO_2	–		–		8×10^{14}	7
O	$<0.1 \times O_2$	1	–		$<10^{13}$	8
Na	4×10^9 at 5 R_E	3	$<1 \times 10^8$ at 3–6 R_G	4	–	
	Na/K = 25 ± 3	3				
K	1.6×10^8 at 5 R_E	3	–		–	
C	–		–		$<2.5\times 10^{13}$	8
H	–		2.4×10^{12}	5	–	

* Numbers in vertical column density, cm^{-2}, unless otherwise noted; (t) = tangential (1) Hall *et al.* 1998; (2) Saur *et al.* 1998; (3) Brown 2001; (4) Brown 1997; (5) Barth *et al.* 1997; Feldman *et al.* 2000a; (6) Kliore *et al.* 2002; (7) Carlson 1999; (8) Strobel *et al.* 2002.

O_2 column densities on Europa and Ganymede inferred by Hall *et al.* (1998).

McCord *et al.* (1997) had previously noted the presence of absorption features in infrared spectra of Ganymede and Callisto that included the 4.26 μm band, which was attributed to CO_2 trapped in fine water ice. This feature appears to be considerably stronger in the detailed mapping spectra of Callisto (Hibbitts *et al.* 2001). This does not necessarily imply a higher abundance of CO_2 on Callisto but may reflect a different nature of the host water ice. However, STIS observations of Ganymede (Feldman *et al.* 2000a) failed to disclose the presence of carbon atoms or any carbon-bearing molecule.

Second, Gurnett *et al.* (2000) have reported *Galileo* plasma wave measurements that imply the presence of electrons with a density almost a thousand times higher than the expected jovian magnetospheric electron density at the orbit of Callisto. This density is comparable with that inferred from similar measurements made in the vicinity of Ganymede. Furthermore, the measurements suggest that the maximum density occurs in the geometric wake of the corotational plasma flow, but not far downstream in an Io-like tail, so one would expect to see a strong trailing/leading hemispherical asymmetry in the atmospheric emissions excited by the plasma electrons. These few measurements could also be interpreted to imply that solar illumination is essential for the presence of the highest plasma densities.

Third, *Galileo* magnetometer measurements (Khurana *et al.* 1998, Kivelson *et al.* 1999) show that Callisto, like Europa, has large-scale magnetic field perturbations characteristic of an induced magnetic dipole field as suggested by Neubauer (1998). For Callisto the perturbation amplitude is equal to the background jovian magnetic field, ~35 nT.

Fourth, a search for UV emissions diagnostic of the presence of O_2, CO_2, and/or CO atmospheres by Strobel *et al.* (2002) yielded only upper limits of 5×10^{-5} photons s^{-1} or 15 R for a uniform disk the diameter of Callisto for emissions of OI λ 1304 Å, OI λ 1356Å, CI λ 1561 Å, CII λ 1335 Å and CO Fourth Positive bands. No useful upper limits on O_2, CO_2, and CO atmospheres, in comparison to the detected CO_2 atmosphere by Carlson (1999) and the inferred O_2 atmosphere by Kliore *et al.* (2002) were derived (see below), but respective upper limits of $\sim 10^{13}$ and 2.5×10^{13} cm^{-2} were placed on atomic carbon and oxygen abundances.

Finally, we note the *Galileo* radio occultation detection of ionospheric electrons with densities up to 2×10^4 cm^{-3} by Kliore *et al.* (2001b), when the necessary geometric configurations of solar illumination and ram angle were met during flybys C20, C22, and C23, when Ψ was $\sim 2°$. These detections imply the presence of a thin, non-uniform atmosphere, which Kliore *et al.* (2002) argue should be O_2, by analogy with Europa, with column density $\sim 3 \times 10^{16}$ cm^{-2} and surface density $\sim 2 \times 10^{10}$ cm^{-3}. These densities are comparable to the densities on Io and almost a factor of 100 times the densities on Europa and Ganymede.

During the *Galileo* flybys with occultations, only C22 yielded plasma wave emissions suitable for extraction of local electron densities (Gurnett *et al.* 2000), but unfortunately these in situ measurements were in the geometric wake on the dark hemisphere side. At closest approach, ~2300 km, no electrons were discernable ($n_e < 0.2\,cm^{-3}$), and further away the torus electron densities were at most 1 cm^{-3} and probably at least an order of magnitude lower. By comparison the ionospheric electron densities measured by radio occultation were ~15 000 cm^{-3} (entry), and ~8000 cm^{-3} (exit) (Kliore *et al.* 2001b), with no detectable wake extension as on Io.

The low torus electron densities imply photoionization is the dominant ionization mechanism in Callisto's atmosphere and in this context Callisto's ionospheric densities are extremely large. It is also surprising that with potentially large $J \times B$ forces the ionospheric plasma is not detectable as it is convected downstream, since even for molecular ions, there is insufficient time for the ionospheric plasma to recombine to densities below the detection threshold of the *Galileo* plasma wave instrument. However, Jupiter's magnetic field is very weak (~35 nT) at Callisto. With Carlson's derived CO_2 atmosphere and the measured electron densities of Kliore *et al.* (2001b), Strobel *et al.* (2002) obtained peak Pedersen and Hall conductivities of ~0.02 and ~0.01 m^{-1} at ~35 and 27 km, respectively. The corresponding peak Pedersen and Hall conductances are ~15 000, and ~7000 mhos. A denser atmosphere due to a larger O_2 component as Kliore *et al.* (2002) infer would not significantly alter these estimates, as the conductivities already maximize above the surface. These conductances are enormous in comparison to the Alfvén conductance, $\Sigma_A \sim 1.3$ mhos and, regardless of the details of the magnetic field line topology close to Callisto, Σ_P and Σ_H are $\gg \Sigma_A$. Strobel *et al.* (2002) estimated that these huge ionospheric conductances result

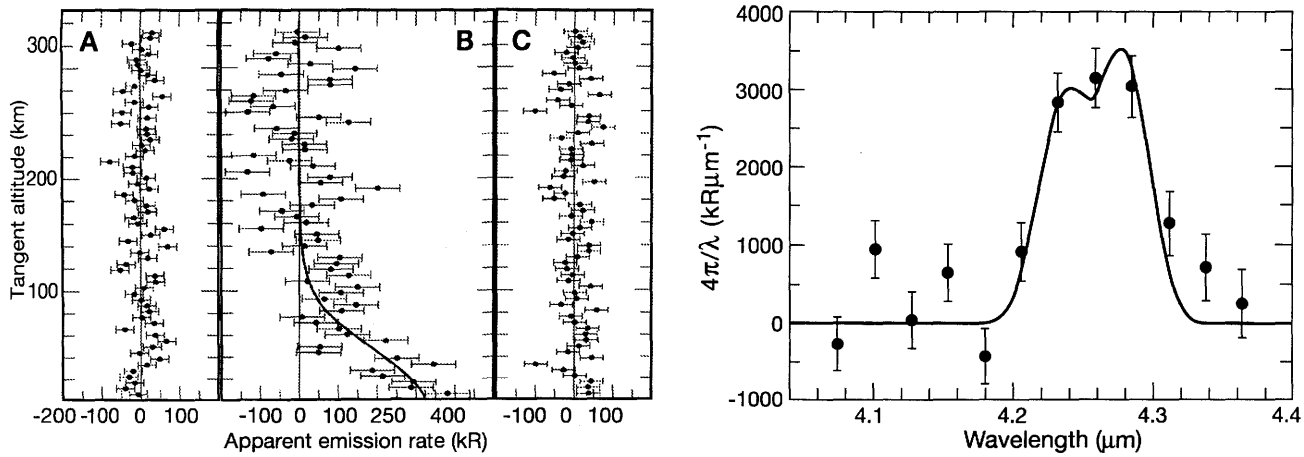

Figure 19.13. The detection of CO_2 emission from Callisto by Carlson (1999).

in $\sim 1.5 \times 10^5$ A flowing through Callisto's ionosphere, which shorts out the corotation electric field yielding a highly reduced ionospheric electric field, and severely retarded ionospheric convection, which increases the $\mathbf{E} \times \mathbf{B}$ plasma transport time constant far in excess of the plasma recombination time constant. The implication is that the observed CO_2 atmosphere can support the observed ionosphere as a static, gravitationally bound plasma impervious to Jupiter's corotational electric field and the associated $\mathbf{E} \times \mathbf{B}$ convection of the ionosphere from the dayside to the nightside and/or off Callisto. The inability to detect UV emission can be understood by this strong electrodynamic interaction with the jovian magnetosphere that reduces the net electron impact emission rate by a factor of $\sim$1500.

In addition, Callisto's ionospheric conductances satisfy the total conductance required by Zimmer *et al.* (2000) to explain the induced magnetic field inferred by Kivelson *et al.* (1999). However, Callisto's ionosphere is transient, present only when the trailing (ram) hemisphere is partially solar illuminated (Kliore *et al.* 2002), and thus cannot be the sole explanation for its induced field. The key remaining problem is the large atmospheric densities ($\sim$40 times the Carlson (1999) CO_2 density) that Kliore *et al.* (2001b) require to explain the inferred ionosphere. With noon temperatures on Callisto of $\sim$150 K, the vapor pressure of H_2O is $\sim 3 \times 10^9\,\mathrm{cm}^{-3}$. The ionization rate of H_2O is $\sim 1.2 \times 10^{-8}\,\mathrm{s}^{-1}$. In photochemical equilibrium with an effective dissociative recombination rate at elevated electron temperatures of $1 \times 10^{-7}\,\mathrm{cm}^{-3}\,\mathrm{s}^{-1}$, the surface electron density would be close to $2 \times 10^4\,\mathrm{cm}^{-3}$. At the terminators the surface temperatures are much colder and a water atmosphere would presumably condense and leave photochemically produced O_2 as the dominant component of the atmosphere. It might be tempting to argue that the terminal ion is Na^+, but like Ganymede, a search for Na atoms at Callisto has given a null result, and no upper limit exists (M. E. Brown 2002, personal communication).

19.4 SUMMARY AND OUTSTANDING QUESTIONS

The Galilean satellites possess tenuous atmospheres with surface pressures ranging from nanobars (SO_2 on Io and the O_2 inferred to be present on Callisto) to picobars (O_2 on Europa and Ganymede; CO_2 on Callisto). A summary of the atmospheric species and their abundances for Io is given in Table 19.2, and for Europa, Ganymede, and Callisto in Table 19.3. Io's atmosphere, with typical SO_2 column densities $>10^{16}\,\mathrm{cm}^{-2}$, is collisionally thick near the equator, but decreases in density toward the poles by more than two orders of magnitude to a collisionally thin value. The distributions of atmospheric species in the atmospheres of Europa, Ganymede, and Callisto are not presently well understood. Despite considerable progress in characterizing the Io atmosphere quantitatively in the past 20 years, and in detecting tenuous atmospheres at the other Galilean satellites, many questions remain.

- Is the predominant source of Io's atmosphere sublimation or volcanoes?
- How variable is Io's atmosphere (both temporally and spatially), and does it drive Io plasma torus variability? What happens to Io's atmosphere at night, and during eclipse?
- What is the relative abundance of O *vs.* O_2 in the Europa and Ganymede atmospheres and how are they distributed spatially?
- Why is Europa's atomic oxygen emission (indicative of its O_2 atmosphere) apparently non-uniform?
- Is the ultimate source of the alkalis at Europa a subsurface ocean?
- What happens to the ionospheric plasma convected downstream at Europa, and why was it not detected by *Galileo* measurements?
- What is the average O_2 atmospheric density at Ganymede? Do the UV and visible oxygen emissions detected at Ganymede have a common (auroral) origin?
- What is the source of Callisto's atmosphere, endogenic or exogenic? Is the major species inferred from the ionospheric measurements O_2, as is presumed?

Acknowledgements. The authors thank Joachim Saur for Fig. 19.10a from Saur *et al.* (1998), Kurt Retherford for Fig. 19.12, and John Spencer for generously sharing prepublication results. DFS was partially supported by NASA

Grant NAG5-12051; REJ was partially supported by NASA Planetary Atmospheres and NSF Astronomy Programs.

REFERENCES

Ballester, G. E., Ultraviolet observations of the atmosphere of Io and the plasma torus, *Ph.D. thesis*, 1989.

Ballester, G. E., H. W. Moos, P. D. Feldman, D. F. Strobel, M. E. Summers, J.-L. Bertaux, T. E. Skinner, M. C. Festou, and J. H. Lieske, Detection of neutral oxygen and sulfur emissions near Io using IUE, *ApJ* **319**, L33–L38, 1987.

Ballester, G. E., D. F. Strobel, H. W. Moos, and P. D. Feldman, The atmospheric abundance of SO_2 on Io, *Icarus* **88**, 1–23, 1990.

Ballester, G. E., M. A. McGrath, D. F. Stobel, X. Zhu, P. D. Feldman, and H. W. Moos, Detection of the SO_2 atmosphere on Io with the Hubble Space Telescope, *Icarus* **111**, 2–17, 1994.

Barth, C. A., C. W. Hord, A. I. F. Stewart, W. R. Pryor, K. E. Simmons, W. E. McClintock, J. M. Ajello, K. L. Naviaux, and J. J. Aiello, *Galileo* ultraviolet spectrometer observations of atomic hydrogen in the atmosphere at Ganymede, *Geophys. Res. Lett.* **24**, 2147–2150, 1997.

Belton, M. J. S., An interpretation of the near-ultraviolet absorption spectrum of SO_2: Implications for Venus, Io, and laboratory measurements, *Icarus* **52**, 149–165, 1982.

Bouchez, A. H., M. E. Brown, and N. M. Schneider, Eclipse spectroscopy of Io's atmosphere, *Icarus* **148**, 316–319, 2000.

Broadfoot, A. L., M. J. Belton, P. Z. Takacs, B. R. Sandel, D. E. Shemansky, J. B. Holberg, J. M. Ajello, H. W. Moos, S. K. Atreya, T. M. Donahue, J. L. Bertaux, J. E. Blamont, D. F. Strobel, J. C. McConnell, R. Goody, A. Dalgarno, and M. B. McElroy, Extreme ultraviolet observations from *Voyager 1* encounter with Jupiter, *Science* **204**, 979–982, 1979.

Broadfoot, A. L., B. R. Sandel, D. E. Shemansky, J. C. McConnell, G. R. Smith, J. B. Holberg, S. K. Atreya, T. M. Donahue, D. F. Strobel, and J. L. Bertaux, Overview of the *voyager* ultraviolet spectrometry results through Jupiter encounter, *J. Geophys. Res.* **86**, 8259–8284, 1981.

Brown, M. E., A Search for a sodium atmosphere around Ganymede, *Icarus* **126**, 236–238, 1997.

Brown, M. E., Potassium in Europa's atmosphere, *Icarus* **151**, 190–195, 2001.

Brown, M. E. and A. H. Bouchez, The response of jupiter's magnetosphere to an outburst on Io, *Science* **278**, 268–271, 1997.

Brown, M. E. and A. H. Bouchez, Observations of Ganymede's visible aurorae, *BAAS* **31**, 1183, 1999.

Brown, M. E. and R. E. Hill, Discovery of an extended sodium atmosphere around Europa, *Nature* **380**, 229–231, 1996.

Brown, R. A., Optical line emission from Io, in *IAU Symp. 65: Exploration of the Planetary System*, pp. 527–531, 1974.

Brown, R. A., The Jupiter hot plasma torus: Observed electron temperature and energy flows, *ApJ* **244**, 1072–1080, 1981.

Brown, W. L., W. M. Augustyniak, L. J. Lanzerotti, R. E. Johnson, and R. Evatt, Linear and nonlinear processes in the erosion of H_2O ice by fast light ions, *Phys. Rev. Lett.* **45**, 1632–1635, 1980.

Burger, M. H., N. M. Schneider, I. de Pater, M. E. Brown, A. H. Bouchez, L. M. Trafton, Y. Sheffer, E. S. Barker, and A. Mallama, Mutual event observations of Io's sodium corona, *ApJ* **563**, 1063–1074, 2001.

Carlson, R. W., A tenuous carbon dioxide atmosphere on Jupiter's moon Callisto, *Science* **283**, 820–821, 1999.

Carlson, R. W., J. C. Bhattacharyya, B. A. Smith, T. V. Johnson, B. Hidayat, S. A. Smith, G. E. Taylor, B. O'Leary, and R. T. Brinkmann, An atmosphere on Ganymede from its occultation of SAO 186800 on 7 June 1972, *Science* **182**, 53–55, 1973.

Chrisey, D. B., R. E. Johnson, J. W. Boring, and J. A. Phipps, Ejection of sodium from sodium sulfide by the sputtering of the surface of Io, *Icarus* **75**, 233–244, 1988.

Clarke, J. T., J. Ajello, J. Luhmann, N. Schneider, and I. Kanik, Hubble Space Telescope UV spectral observations of Io passing into eclipse, *J. Geophys. Res.* **99**, 8387–8402, 1994.

Combi, M. R., K. Kabin, T. I. Gombosi, D. L. Dezeeuw, and K. G. Powell, Io's plasma environment during the *Galileo* flyby: Global three-dimensional MHD modeling with adaptive mesh refinement, *J. Geophys. Res.* **103**, 9071–9082, 1998.

Cook, A. F., E. M. Shoemaker, B. A. Smith, G. E. Danielson, T. V. Johnson, and S. P. Synnott, Volcanic origin of the eruptive plumes on Io, *Science* **211**, 1419–1422, 1981.

Cooper, J. F., R. E. Johnson, B. H. Mauk, H. B. Garrett, and N. Gehrels, Energetic ion and electron irradiation of the icy Galilean satellites, *Icarus* **149**, 133–159, 2001.

de Pater, I., H. Roe, J. R. Graham, D. F. Strobel, and P. Bernath, Detection of the forbidden SO $a^1\Delta - X^3\Sigma^-$ rovibronic transition on Io at 1.7 μm, *Icarus* **156**, 296–301, 2002.

Doering, J. P. and J. Yang, Atomic oxygen ^3P–$^3S^o$ (λ1304 Å) transition revisited: Cross section near threshold, *J. Geophys. Res.* **106**, 203–210, 2001.

Douté, S., B. Schmitt, R. Lopes-Gautier, R. Carlson, L. Soderblom, J. Shirley, and the *Galileo* NIMS Team, Mapping SO_2 frost on Io by the modeling of NIMS hyperspectral images, *Icarus* **149**, 107–132, 2001.

Durrance, S. T., P. D. Feldman, and H. A. Weaver, Rocket detection of ultraviolet emission from neutral oxygen and sulfur in the Io torus, *ApJ* **267**, L125–L129, 1983.

Eviatar, A., A. Bar-Nun, and M. Podolak, Europan surface phenomena, *Icarus* **61**, 185–191, 1985.

Eviatar, A., D. F. Strobel, B. C. Wolven, P. D. Feldman, M. A. McGrath, and D. J. Williams, Excitation of the Ganymede ultraviolet aurora, *ApJ* **555**, 1013–1019, 2001.

Fanale, F. P., T. V. Johnson, and D. L. Matson, Io: A surface evaporite deposit, *Science* **186**, 922–925, 1974.

Fanale, F. P., R. H. Brown, D. P. Cruikshank, and R. N. Clake, Significance of absorption features in Io's IR reflectance spectrum, *Nature* **280**, 761–763, 1979.

Fanale, F. P., W. B. Banerdt, L. S. Elson, T. V. Johnson, and R. W. Zurek, Io's surface: Its phase composition and influence on Io's atmosphere and Jupiter's magnetosphere, in *Satellites of Jupiter*, pp. 756–781, 1982.

Feaga, L. M., M. A. McGrath, P. D. Feldmon and D. F. Strobel, Detection of atomic chlorine in Io's atmosphere with HST/GHRS, *Ap. J.* **in press**, 2004.

Feaga, L. M., M. A. McGrath, and P. D. Feldman, The Abundance of atomic sulfur in the atmosphere of Io, *ApJ* **570**, 439–446, 2002.

Fegley, B. and M. Y. Zolotov, Chemistry of sodium, potassium, and chlorine in volcanic gases on Io, *Icarus* **148**, 193–210, 2000.

Feldman, P. D., M. A. McGrath, D. F. Strobel, H. W. Moos, K. D. Retherford, and B. C. Wolven, HST/STIS ultraviolet imaging of polar aurora on Ganymede, *ApJ* **535**, 1085–1090, 2000a.

Feldman, P. D., D. F. Strobel, H. W. Moos, K. D. Retherford, B. C. Wolven, M. A. McGrath, F. L. Roesler, R. C. Woodward, R. J. Oliversen, and G. E. Ballester, Lyman-α imaging of the SO_2 distribution on Io, *Geophys. Res. Lett.* **27**, 1787, 2000b.

Gehrels, T., ed., *Jupiter*, University of Arizona Press, 1976.

Geissler, P. E., A. S. McEwen, W. Ip, M. J. Belton, T. V. Johnson, W. H. Smyth, and A. P. Ingersoll, *Galileo* imaging of atmospheric emissions from Io, *Science* **285**, 870–874, 1999.

Goertz, C. K., Io's interaction with the plasma torus, *J. Geophys. Res.* **85**, 2949–2956, 1980.

Goguen, J. D. and D. L. Blaney, Io's 1–2.5 μm spectrum in eclipse with SpeX at IRTF, *BAAS* **33**, 2402, 2001.

Gurnett, D. A., W. S. Kurth, A. Roux, S. J. Bolton, E. A. Thomsen, and J. B. Groene, *Galileo* plasma wave observations near Europa, *Geophys. Res. Lett.* **25**, 237, 1998.

Gurnett, D. A., A. M. Persoon, W. S. Kurth, A. Roux, and S. J. Bolton, Plasma densities in the vicinity of Callisto from *Galileo* plasma wave observations, *Geophys. Res. Lett.* **27**, 1867, 2000.

Gurnett, D. A., A. M. Persoon, W. S. Kurth, A. Roux, and S. J. Bolton, Electron densities near Io from *Galileo* plasma wave observations, *J. Geophys. Res.* **106**, 26 225–26 232, 2001.

Hall, D. T., D. F. Strobel, P. D. Feldman, M. A. McGrath, and H. A. Weaver, Detection of an oxygen atmosphere on Jupiter's moon Europa, *Nature* **373**, 677, 1995.

Hall, D. T., P. D. Feldman, M. A. McGrath, and D. F. Strobel, The far-ultraviolet oxygen airglow of Europa and Ganymede, *ApJ* **499**, 475, 1998.

Hanel, R., B. Conrath, M. Flasar, L. Herath, V. Kunde, P. Lowman, W. Maguire, J. Pearl, J. Pirraglia, and L. Horn, Infrared observations of the jovian system from *Voyager 2*, *Science* **206**, 952–956, 1979.

Hendrix, A. R., C. A. Barth, and C. W. Hord, Io's patchy SO_2 atmosphere as measured by the *Galileo* ultraviolet spectrometer, *J. Geophys. Res.* **104**, 11 817–11 826, 1999.

Hibbitts, C. A., R. Pappalardo, J. Klemaszewski, T. B. McCord, and G. B. Hansen, Comparing carbon dioxide distributions on Ganymede and Callisto, in *Lunar and Planetary Science Conference Abstracts*, pp. 1263, 2001.

Hinson, D. P., A. J. Kliore, F. M. Flasar, J. D. Twicken, P. J. Schinder, and R. G. Herrera, *Galileo* radio occultation measurements of Io's ionosphere and plasma wake, *J. Geophys. Res.* **103**, 29 343–29 357, 1998.

Ingersoll, A. P., Io meteorology: How atmospheric pressure is controlled locally by volcanos and surface frosts, *Icarus* **81**, 298–313, 1989.

Ingersoll, A. P., M. E. Summers, and S. G. Schlipf, Supersonic meteorology of Io: Sublimation-driven flow of SO_2, *Icarus* **64**, 375–390, 1985.

Ip, W.-H., Europa's oxygen exosphere and its magnetospheric interaction, *Icarus* **120**, 317–325, 1996.

Jessup, K. L., J. R. Spencer, G. E. Ballester, R. Howell, F. Roessler, M. Vigil, and R. Yelle, The atmospheric signature of Io's Prometheus Plume and anti-jovian hemisphere: Evidence for a sublimation atmosphere, *Icarus* **submitted**, 2004.

Johnson, R. E., Application of laboratory data to the sputtering of a planetary regolith, *Icarus*, **78**, 206–210, 1989.

Johnson, R. E., Formation of Na-containing molecular ions at Io, *Icarus* **111**, 65–72, 1994.

Johnson, R. E., Sodium at Europa, *Icarus* **143**, 429–433, 2000.

Johnson, R. E., Surface chemistry in the jovian magnetosphere radiation environment, in *Chemical Dynamics in Extreme Envionments*, R. Dressler, ed., pp. 390–419, World Scientific, 2001.

Johnson, R. E., L. J. Lanzerotti, and W. L. Brown, Planetary applications of ion induced erosion of condensed gas frosts, *Nucl. Inst. Meth. Phys. Res. A* **198**, 147–158, 1982.

Johnson, R. E., J. W. Boring, C. T. Reimann, L. A. Barton, J. W. Sieveka, J. W. Garrett, K. R. Farmer, W. L. Brown, and L. J. Lanzerotti, Plasma ion-induced molecular ejection on the Galilean satellites: Energies of ejected molecules, *Geophys. Res. Lett.* **10**, 892–895, 1983.

Johnson, R. E., F. Leblanc, B. V. Yakshinskiy, and T. E. Madey, Energy distributions for desorption of sodium and potassium from ice: The Na/K ratio at Europa, *Icarus* **156**, 136–142, 2002.

Johnson, T. V. and D. L. Matson, Io's tenuous atmosphere, in *Origin and Evolution of Planetary and Satellite Atmospheres*, A. K. Atreya, J. B. Pollack, M. S. Matthews (eds), University of Arizona Press, pp. 666–681, 1989.

Johnson, T. V., D. L. Matson, D. L. Blaney, G. J. Veeder, and A. Davies, Stealth plumes on Io, *Geophys. Res. Lett.* **22**, 3293, 1995.

Johnson, R. E., M. Liu, and C. Tully, Collisional dissociations cross sections for $O+O_2$, CO and N_2, O_2+O_2, $N+N_2$ and N_2+N_2, *Planet. Space Sci.*, **50**, 123–128, 2002.

Kargel, J. S., Brine volcanism and the interior structures of asteroids and icy satellites, *Icarus* **94**, 368–390, 1991.

Kerton, C. R., F. P. Fanale, and J. R. Salvail, The state of SO_2 on Io's surface, *J. Geophys. Res.* **101**, 7555–7564, 1996.

Khurana, K. K., M. G. Kivelson, D. J. Stevenson, G. Schubert, R. J. Russell, C. T.and Walker, and C. Polanskey, Induced magnetic fields as evidence for subsurface oceans in Europa and Callisto, *Nature* **395**, 777–780, 1998.

Kieffer, S. W., Dynamics and thermodynamics of volcanic eruptions: Implications for the plumes on Io, in *Satellites of Jupiter*, pp. 647–723, 1982.

Kivelson, M. G., K. K. Khurana, C. T. Russell, R. J. Walker, J. Warnecke, F. V. Coroniti, C. Polanskey, D. J. Southwood, and G. Schubert, Discovery of Ganymede's magnetic field by the *Galileo* spacecraft, *Nature* **384**, 537–541, 1996.

Kivelson, M. G., K. K. Khurana, F. V. Coroniti, S. Joy, C. T. Russell, R. J. Walker, J. Warnecke, L. Bennett, and C. Polanskey, Magnetic field and magnetosphere of Ganymede, *Geophys. Res. Lett.* **24**, 2155, 1997.

Kivelson, M. G., K. K. Khurana, D. J. Stevenson, L. Bennett, S. Joy, C. T. Russell, R. J. Walker, C. Zimmer, and C. Polanskey, Europa and Callisto: Induced or intrinsic fields in a periodically varying plasma environment, *J. Geophys. Res.* **104**, 4609–4626, 1999.

Kliore, A., D. L. Cain, G. Fjeldbo, B. L. Seidel, and S. I. Rasool, Preliminary results on the atmospheres of Io and Jupiter from the *Pioneer 10* S-Band occultation experiment, *Science* **183**, 323–324, 1974.

Kliore, A. J., G. Fjeldbo, B. L. Seidel, D. N. Sweetnam, T. T. Sesplaukis, P. M. Woiceshyn, and S. I. Rasool, The atmosphere of Io from *Pioneer 10* radio occultation measurements, *Icarus* **24**, 407–410, 1975.

Kliore, A. J., D. P. Hinson, F. M. Flasar, A. F. Nagy, and T. E. Cravens, The ionosphere of Europa from *Galileo* radio occultations, *Science* **277**, 355–358, 1997.

Kliore, A. J., A. Anabtawi, and A. F. Nagy, The ionospheres of Europa, Ganymede, and Callisto, *Eos*, p. B506, 2001a.

Kliore, A. J., A. Anabtawi, A. F. Nagy, and *Galileo* Radio Propagation Science Team, The ionospheres of Ganymede and Callisto from *Galileo* radio occultations, *BAAS* **33**, 1084, 2001b.

Kliore, A. J., A. Anabtawi, R. G. Herrera, S. W. Asmar, A. F. Nagy, D. P. Hinson, and F. M. Flasar, The ionosphere of Callisto from *Galileo* radio occultation observations, *J. Geophys. Res.* **107**, pp. SIA 19–1, 2002.

Kuiper, G. P., Infrared observations of planets and satellites, *AJ* **62**, 245, 1957.

Kumar, S., Photochemistry of SO_2 in the atmosphere of Io and implications on atmospheric escape, *J. Geophys. Res.* **87**, 1677–1684, 1982.

Kumar, S., The SO_2 atmosphere and ionosphere of Io: Ion chemistry, atmospheric escape, and models corresponding to the *Pioneer 10* radio occultation measurements, *Icarus* **61**, 101–123, 1985.

Kumar, S. and D. M. Hunten, The atmospheres of Io and other satellites, in *Satellites of Jupiter*, D. Morrison (ed), University of Arizona Press, pp. 782–806, 1982.

Kupo, I., Y. Mekler, and A. Eviatar, Detection of ionized sulfur in the jovian magnetosphere, *ApJ* **205**, L51–L53, 1976.

Kurth, W. S., D. A. Gurnett, A. M. Persoon, A. Roux, S. J. Bolton, and C. J. Alexander, The plasma wave environment of Europa, *Planet. Space Sci.* **49**, 345–363, 2001.

Lanzerotti, L. J., W. L. Brown, J. M. Poate, and W. M. Augustyniak, On the contribution of water products from Galilean satellites to the jovian magnetosphere, *Geophys. Res. Lett.* **5**, 155–158, 1978.

Leblanc, F., R. E. Johnson, and M. E. Brown, Europa's sodium atmosphere: An ocean source?, *Icarus* **159**, 132–144, 2002.

Lellouch, E., Io's atmosphere: Not yet understood, *Icarus* **124**, 1–21, 1996.

Lellouch, E., T. Encrenaz, M. Belton, I. de Pater, and S. Gulkis, Io's atmosphere from microwave detection SO_2, *Nature* **346**, 639–641, 1990.

Lellouch, E., M. Belton, I. de Pater, G. Paubert, S. Gulkis, and T. Encrenaz, The structure, stability, and global distribution of Io's atmosphere, *Icarus* **98**, 271–295, 1992.

Lellouch, E., D. F. Strobel, M. J. Belton, M. E. Summers, G. Paubert, and R. Moreno, Detection of sulfur monoxide in Io's atmosphere, *ApJ* **459**, L107–L110, 1996.

Lellouch, E., G. Paubert, D. F. Strobel, and M. Belton, Millimeter-wave observations of Io's atmosphere: The IRAM 1999 campaign, *BAAS* **32**, 3511, 2000.

Lellouch, E., G. Paubert, J. I. Moses, N. M. Schneider, and D. F. Strobel, Volcanically emitted sodium chloride as a source for Io's neutral clouds and plasma torus, *Nature* **421**, 45–47, 2003.

Lewis, J. S., Satellites of the outer planets: Their physical and chemical nature, *Icarus* **15**, 174, 1971.

Linker, J. A., K. K. Khurana, M. G. Kivelson, and R. J. Walker, MHD simulations of Io's interaction with the plasma torus, *J. Geophys. Res.* **103**, 19 867–19 878, 1998.

Lopes-Gautier, R., A. S. McEwen, W. B. Smythe, P. E. Geissler, L. Kamp, A. G. Davies, J. R. Spencer, L. Keszthelyi, R. Carlson, F. E. Leader, R. Mehlman, L. Soderblom, and the *Galileo* NIMS and SSI Teams, Active volcanism on Io: Global distribution and variations in activity, *Icarus* **140**, 243–264, 1999.

Madey, T. E., B. V. Yakshinskiy, V. N. Ageev, and R. E. Johnson, Desorption of alkali atoms and ions from oxide surfaces: Relevance to origins of Na and K in atmospheres of Mercury and the Moon, *J. Geophys. Res.* **103**, 5873, 1998.

Manat, S. L. and A. L. Lane, A compilation of the absorption cross-sections of SO_2 from 106 to 403 nm, *J. Quant. Spectrosc. Radiat. Transf.*, **50**, 267–276, 1993.

Matson, D. L. and D. B. Nash, Io's atmosphere: Pressure control by regolith cold trapping and surface venting, *J. Geophys. Res.* **88**, 4771–4783, 1983.

Matson, D. L., T. V. Johnson, and F. P. Fanale, Sodium d-line emission from Io: Sputtering and resonant scattering hypothesis, *ApJ* **192**, L43, 1974.

McCord, T. B., R. Carlson, W. Smythe, G. Hansen, R. Clark, C. Hibbitts, F. Fanale, J. Granahan, M. Segura, D. Matson, T. Johnson, and P. Martin, Organics and other molecules in the surfaces of Callisto and Ganymede, *Science* **278**, 271–275, 1997.

McEwen, A. S., L. A. Soderblom, T. V. Johnson, and D. L. Matson, The global distribution, abundance, and stability of SO_2 on Io, *Icarus* **75**, 450–478, 1988.

McGrath, M. A. and R. E. Johnson, Magnetospheric plasma sputtering of Io's atmosphere, *Icarus*, **69**, 519–531, 1987.

McGrath, M. A., M. J. S. Belton, J. R. Spencer, and P. Sartoretti, Spatially resolved spectroscopy of Io's Pele Plume and SO_2 atmosphere, *Icarus* **146**, 476–493, 2000a.

McGrath, M. A., P. D. Feldman, D. F. Strobel, K. Retherford, B. Wolven, and H. W. Moos, HST/STIS ultraviolet imaging of Europa, *BAAS* **32**, 1056, 2000b.

Mendillo, M., J. Baumgardner, B. Flynn, and W. J. Hughes, The extended sodium nebula of Jupiter, *Nature* **348**, 312–314, 1990.

Morabito, L. A., S. P. Synnott, P. N. Kupferman, and S. A. Collins, Discovery of currently active extraterrestrial volcanism, *Science* **204**, 972, 1979.

Moreno, M. A., G. Schubert, M. G. Kivelson, D. A. Paige, and J. Baumgardner, Io's volcanic and sublimation atmospheres, *Icarus* **93**, 63–81, 1991.

Moroz, V. I., On the infrared spectra of Jupiter and Saturn (0.9–2.5 μ), *AZh* **38**, 1080, 1961.

Moses, J. I., M. Y. Zolotov, and B. Fegley, Alkali and chlorine photochemistry in a volcanically driven atmosphere on Io, *Icarus* **156**, 107–135, 2002a.

Moses, J. I., M. Y. Zolotov, and B. Fegley, Photochemistry of a volcanically driven atmosphere on Io: Sulfur and oxygen species from a Pele-type eruption, *Icarus* **156**, 76–106, 2002b.

Ness, N. F., M. H. Acuna, R. P. Lepping, L. F. Burlaga, K. W. Behannon, and F. M. Neubauer, Magnetic field studies at Jupiter by *Voyager 1*: Preliminary results, *Science* **204**, 982–987, 1979.

Neubauer, F. M., Nonlinear standing Alfven wave current system at Io: Theory, *J. Geophys. Res.* **85**, 1171–1178, 1980.

Neubauer, F. M., The sub-Alfvénic interaction of the Galilean satellites with the jovian magnetosphere, *J. Geophys. Res.* **103**, 19 843, 1998.

Noren, C., I. Kanik, J. M. Ajello, P. McCartney, O. P. Makarov, W. E. McClintock, and V. A. Drake, Emission cross section of OI (135.6 nm) at 100 eV resulting from electron-impact dissociative excitation of O_2, *Geophys. Res. Lett.* **28**, 1379, 2001.

Oliversen, R. J., F. Scherb, W. H. Smyth, M. E. Freed, R. Carey Woodward, M. L. Marconi, K. D. Retherford, O. L. Lupie, and J. P. Morgenthaler, Sunlit Io atmospheric [OI] 6300 Å emission and the plasma torus, *J. Geophys. Res.* **106**, 26 183–26 194, 2001.

Paranicas, C., R. W. Carlson, and R. E. Johnson, Electron bombardment of Europa, *Geophys. Res. Lett.* **28**, 673, 2001.

Paranicas, C. P., M. Volwerk, and M. G. Kivelson, Flow diversion at Europa, in *Eos*, pp. P21B–07, 2002.

Paresce, F., P. Sartoretti, R. Albrecht, C. Barbieri, J. C. Blades, A. Boksenberg, P. Crane, J. M. Deharveng, M. J. Disney, and P. Jakobsen, Near-ultraviolet imaging of Jupiter's satellite Io with the Hubble Space Telescope, *A&A* **262**, 617–620, 1992.

Paterson, W. R., L. A. Frank, and K. L. Ackerson, *Galileo* plasma observations at Europa: Ion energy spectra and moments, *J. Geophys. Res.* **104**, 22 779–22 792, 1999.

Pearl, J., R. Hanel, V. Kunde, W. Maguire, K. Fox, S. Gupta, C. Ponnamperuma, and F. Raulin, Identification of gaseous SO_2 and new upper limits for other gases on Io, *Nature* **280**, 755–758, 1979.

Pilcher, C. B., S. T. Ridgway, and T. B. McCord, Galilean satellites: Identification of water frost, *Science* **178**, 1087–1089, 1972.

Retherford, K. D., *Io's Aurora: HST/STIS Observations*, Ph.D. thesis , 2002.

Retherford, K. D., P. D. Feldman, H. W. Moos, D. F. Strobel, B. C. Wolven, R. J. Oliversen, M. A. McGrath, F. L. Roesler, F. Scherb, G. E. Ballester, W. H. Smyth, and F. Bagenal, Io's UV aurora: Detection of neutral hydrogen and neutral chlorine, *BAAS* **32**, 1055, 2000.

Roesler, F. L., H. W. Moos, R. J. Oliversen, J. C. Woodward, R., K. D. Retherford, F. Scherb, M. A. McGrath, W. H. Smyth, P. D. Feldman, and D. F. Strobel, Far-ultraviolet imaging spectroscopy of Io's atmosphere with HST/STIS, *Science* **283**, 353, 1999.

Sartoretti, P., M. A. McGrath, and F. Paresce, Disk-resolved imaging of Io with the Hubble Space Telescope, *Icarus* **108**, 272–284, 1994.

Sartoretti, P., M. J. S. Belton, and M. A. McGrath, SO_2 distributions on Io, *Icarus* **122**, 273–287, 1996.

Saur, J., D. F. Strobel, and F. M. Neubauer, Interaction of the jovian magnetosphere with Europa: Constraints on the neutral atmosphere, *J. Geophys. Res.* **103**, 19 947, 1998.

Saur, J., F. M. Neubauer, D. F. Strobel, and M. E. Summers, Three-dimensional plasma simulation of Io's interaction with the Io plasma torus: Asymmetric plasma flow, *J. Geophys. Res.* **104**, 25 105–25 126, 1999.

Saur, J., F. M. Neubauer, D. F. Strobel, and M. E. Summers, Io's ultraviolet aurora: Remote sensing of Io's interaction, *Geophys. Res. Lett.*, **27**, 2893, 2000.

Saur, J., F. M. Neubauer, D. F. Strobel, and M. E. Summers, Interpretation of Galileo's Io plasma and field observations: I0, I24, and I27 flybys and close polar passes, *J. Geophys. Res.*, **107**, 1422, 2002.

Schmitt, B., C. de Bergh, E. Lellouch, J. Maillard, A. Barbe, and S. Doute, Identification of three absorption bands in the 2-μm spectrum of Io, *Icarus* **111**, 79–105, 1994.

Schmitt, B., S. Rodriguez, and NIMS/*Galileo* Team, Cl_2SO_2 deposits near the Marduk's volcanic center on Io, *BAAS* **33**, 1073, 2001.

Schneider, N. M., D. M. Hunten, W. K. Wells, A. B. Schultz, and U. Fink, The structure of Io's corona, *ApJ* **368**, 298–315, 1991.

Scudder, J. D., E. C. Sittler, and H. S. Bridge, A survey of the plasma electron environment of Jupiter: A view from *Voyager*, *J. Geophys. Res.* **86**, 8157–8179, 1981.

Shematovich, V. I. and R. E. Johnson, Near-surface oxygen atmosphere at Europa, *Adv. Space Res.* **27**, 1881–1888, 2001.

Shematovich, V. I., R. E. Johnson, J. F. Cooper, and M. C. Wong, Surface-bounded atmosphere of Europa, *Icarus*, **submitted**, 2004.

Shi, M., R. A. Baragiola, D. E. Grosjean, R. E. Johnson, S. Jurac, and J. Schou, Sputtering of water ice surfaces and the production of extended neutral atmospheres, *J. Geophys. Res.* **100**, 26 387–26 396, 1995.

Smyth, W. H. and M. R. Combi, A general model for Io's neutral gas clouds: II. Application to the sodium cloud, *ApJ* **328**, 888–918, 1988.

Smyth, W. H. and M. R. Combi, Io's sodium corona and spatially extended cloud: A consistent flux speed distribution, *Icarus* **126**, 58–77, 1997.

Smyth, W. H. and M. L. Marconi, Io's oxygen source: Determination from ground-based observations and implications for the plasma torus, *J. Geophys. Res.* **105**, 7783–7792, 2000.

Smythe, W. D., R. M. Nelson, and D. B. Nash, Spectral evidence for SO_2 frost or adsorbate on Io's surface, *Nature* **280**, 766, 1979.

Spencer, J. R., Icy Galilean satellite reflectance spectra: Less ice on Ganymede and Callisto?, *Icarus* **70**, 99–110, 1987.

Spencer, J. R. and N. M. Schneider, Io on the Eve of the *Galileo* mission, *Ann. Rev. Earth Planet. Sci.* **24**, 125–190, 1996.

Spencer, J. R., P. Sartoretti, G. E. Ballester, A. S. McEwen, J. T. Clarke, and M. A. McGrath, Pele plume (Io): Observations with the Hubble Space Telescope, *Geophys. Res. Lett.* **24**, 2471, 1997.

Spencer, J. R., K. L. Jessup, M. A. McGrath, G. E. Ballester, and R. Yelle, Discovery of gaseous S_2 in Io's Pele Plume, *Science* **288**, 1208–1210, 2000.

Spencer, J. R., K. L. Jessup, E. Lellouch, M. Richter, T. Greathouse, M. Lopez-Valverde, and J.-M. Flaud, Ground-based infrared detection of Io's SO_2 atmosphere, *BAAS* **34**, 912, 2002.

Strobel, D. F. and B. C. Wolven, The atmosphere of Io: Abundances and sources of sulfur dioxide and atomic hydrogen, *Ap&SS* **277**, 271–287, 2001.

Strobel, D. F., X. Zhu, and M. F. Summers, On the vertical thermal structure of Io's atmosphere, *Icarus* **111**, 18–30, 1994.

Strobel, D. F., J. Saur, P. D. Feldman, and M. A. McGrath, Hubble Space Telescope Space Telescope Imaging Spectrograph search for an atmosphere on Callisto: A jovian unipolar inductor, *ApJ* **581**, L51–L54, 2002.

Summers, M. E., *Theoretical Studies of Io's Atmosphere*, Ph.D. thesis, California Institute of Technology, 1985.

Summers, M. E. and D. F. Strobel, Photochemistry and vertical transport in Io's atmosphere and ionosphere, *Icarus* **120**, 290–316, 1996.

Trafton, L., Detection of a potassium cloud near Io, *Nature* **258**, 690–692, 1975.

Trafton, L. M., J. J. Caldwell, C. Barnet, and C. C. Cunningham, The gaseous sulfur dioxide abundance over Io's leading and trailing hemispheres: HST spectra of Io's C 1B 2–X 1A 1 band of SO_22 near 2100 angstrom, *ApJ* **456**, 384, 1996.

Trafton, L. M., D. L. Matson, and J. A. Stansberry, Surface/atmosphere interactions and volatile transport (Triton, Pluto and Io), in ASSL, vol. 227, *Solar System Ices*, pp. 773, 1998.

Veeder, G. J., D. L. Matson, T. V. Johnson, D. L. Blaney, and J. D. Goguen, Io's heat flow from infrared radiometry: 1983–1993, *J. Geophys. Res.*, **99**, 17,095–17,162, 1994.

Wiens, R. C., D. S. Burnett, W. F. Calaway, C. S. Hansen, K. R. Lykke, and M. J. Pellin, Sputtering products of sodium sulfate: Implications for Io's surface and for sodium-bearing molecules in the Io torus, *Icarus* **128**, 386–397, 1997.

Wilson, J. K. and N. M. Schneider, Io's fast sodium: Implications for molecular and atomic atmospheric escape, *Icarus* **111**, 31–44, 1994.

Wilson, J. K. and N. M. Schneider, Io's sodium directional feature: Evidence for ionospheric escape, *J. Geophys. Res.* **104**, 16 567–16 584, 1999.

Wilson, J. K., M. Mendillo, J. Baumgardner, N. M. Schneider, J. T. Trauger, and B. Flynn, The dual sources of Io's sodium clouds, *Icarus* **in press**, 2003.

Wolff, R. S. and D. A. Mendis, On the nature of the interaction of the jovian magnetosphere with the icy Galilean satellites, *J. Geophys. Res.* **88**, 4749–4769, 1983.

Wolven, B. C., H. W. Moos, K. D. Retherford, P. D. Feldman, D. F. Strobel, W. H. Smyth, and F. L. Roesler, Emission profiles of neutral oxygen and sulfur in Io's exospheric corona, *J. Geophys. Res.* **106**, 26 155–26 182, 2001.

Wong, M. C. and R. E. Johnson, The effect of plasma heating on sublimation-driven flow in Io's atmosphere, *Icarus* **115**, 109–118, 1995.

Wong, M. C. and R. E. Johnson, A three-dimensional azimuthally symmetric model atmosphere for Io: 1. Photochemistry and the accumulation of a nightside atmosphere, *J. Geophys. Res.* **101**, 23 243–23 254, 1996a.

Wong, M. C. and R. E. Johnson, A three-dimensional azimuthally symmetric model atmosphere for Io: 2. Plasma effect on the surface, *J. Geophys. Res.* **101**, 23 255–23 260, 1996b.

Wong, M. C. and W. H. Smyth, Model calculations for Io's atmosphere at eastern and western elongations, *Icarus* **146**, 60–74, 2000.

Wu, R. C. Y., B. W. Yang, F. Z. Chen, D. L. Judge, J. Caldwell, and L. M. Trafton, Measurements of high-, room-, and low-temperature photoabsorption cross sections of SO_2 in the 2080- to 2950-Å region, with application to Io, *Icarus* **145**, 289–296, 2000.

Yakshinskiy, B. V. and T. E. Madey, Photon-stimulated desorption as a substantial source of sodium in the lunar atmosphere, *Nature* **400**, 642–644, 1999.

Yakshinskiy, B. V. and T. E. Madey, Electron- and photon-stimulated desorption of K from ice surfaces, *J. Geophys. Res.* **106**, 33 303–33 308, 2001.

Yung, Y. L. and M. B. McElroy, Stability of an oxygen atmosphere on Ganymede, *Icarus* **30**, 97–103, 1977.

Zhang, J., D. B. Goldstein, P. L. Varghese, N. E. Gimelshein, S. F. Gimelshein, and D. A. Levin, Simulation of gas dynamics and radiation in volcanic plumes on Io, *Icarus* **163**, 182–197, 2003.

Zimmer, C., K. K. Khurana, and M. G. Kivelson, Subsurface oceans on Europa and Callisto: Constraints from *Galileo* magnetometer observations, *Icarus* **147**, 329–347, 2000.

Zolotov, M. Y. and B. Fegley, Volcanic origin of disulfur monoxide (S_2O) on Io, *Icarus* **133**, 293–297, 1998a.

Zolotov, M. Y. and B. Fegley, Volcanic production of sulfur monoxide (SO) on Io, *Icarus* **132**, 431–434, 1998b.

Zolotov, M. Y. and B. Fegley, Oxidation state of volcanic gases and the interior of Io, *Icarus* **141**, 40–52, 1999.

Zolotov, M. Y. and B. J. Fegley, Eruption conditions of Pele volcano on Io inferred from chemistry of its volcanic plume, *Geophys. Res. Lett.* **27**, 2789, 2000.

Zolotov, M. Y. and E. L. Shock, Geochemical constraints on the oxidation states of the europan ocean and mantle, in *Lunar and Planetary Science Conference Abstracts*, p. 2025, 2001.